Hydrolysis of organometallic and metal-amide precursors: Synthesis routes to oxo-bridged heterometallic complexes, metal-oxo clusters and metal oxide nanoparticles

Dalton Transactions

Accepted Manuscript

This article can be cited before page numbers have been issued, to do this please use: S. D. Pike and J. A. Garden, *Dalton Trans.*, 2018, DOI: 10.1039/C8DT00017D.

ROYAL SOCIETY OF CHEMISTRY

rsc.li/dalton

View Article Online
DOI: 10.1039/C8DT00017D

Journal Name

ARTICLE

Hydrolysis of organometallic and metal-amide precursors: Synthesis routes to oxo-bridged heterometallic complexes, metal-oxo clusters and metal oxide nanoparticles

Received 00th January 20xx,
Accepted 00th January 20xx

DOI: 10.1039/x0xx00000x

www.rsc.org/

J. A. Garden,*[a] S. D. Pike*[b]

The hydrolysis reaction between Brønsted basic organometallic or metal-amide reagents with Brønsted acidic OH groups from water or metal-hydroxides may act as a controlled stoichiometric strategy for the formation of M–O–M bonds, if careful consideration of reaction conditions is employed. This article explores the utilisation of highly reactive organometallic and metal-amide complexes from across the periodic table as reagents for the synthesis of metal-oxo clusters, oxo-bridged heterobimetallics and metal oxide nanoparticles. Such reactivity typically occurs at low temperatures with the release of hydrocarbon or amine by-products. The impact of ligand coordination, M–C bond strength, M–OH acidity and reaction temperature are discussed.

1. Introduction

In the laboratory much time and effort is spent keeping water molecules outside of the reaction flask, especially when highly reactive metal complexes are used. It is commonly recognised that organometallics (such as $ZnEt_2$) or metal-amides [such as $Fe(N(SiMe_3)_2)_2$] react rapidly with moisture to form the respective metal oxide materials. However, such potent reactivity can be advantageous if the source and stoichiometry of water is carefully controlled and the reaction conditions (e.g. temperature and speed of addition) are carefully considered. By harnessing this ability to craft metal-oxygen-metal connectivity a range of desirable metal-oxygen molecular species, nanoparticles (NPs) and materials may be generated in a controlled manner. This perspective will examine synthetic routes to form (mixed) metal-oxo molecular clusters and NPs using reactive metal species, focussing on the reaction of organometallics (MR_x) and metal-amides ($M(NR_2)_x$) with protic reagents such as water or metal-hydroxides.

1.i Preparation and applications of metal oxides

The simple combination of metal cations with oxide anions produces a host of remarkable materials with applications spanning ceramics, semiconductors and magnetic materials.[1, 2] Titanium dioxide is used in sun creams, solar cells and self-cleaning windows;[3, 4] zinc oxide has antibacterial properties, and is used in varistors;[5] and indium tin oxide is a transparent conductor allowing for touch screen technology in modern

[a] EaStCHEM School of Chemistry, University of Edinburgh, Edinburgh EH9 3FJ, UK
[b] Department of Chemistry, University of Cambridge, Cambridge, CB2 1EW, UK

Jennifer A. Garden

Jennifer A. Garden received her PhD in organometallic chemistry from the University of Strathclyde in 2014, supervised by Prof. Robert Mulvey. This was followed by two years of post-doctoral research at Imperial College London, where she developed polymerisation catalysts with Prof. Charlotte Williams. In 2016, she returned to Scotland to take up the first Christina Miller Fellowship at the University of Edinburgh. Work in the Garden group currently focuses on the design and synthesis of novel homo- and heterobimetallic compounds, and their application towards homogeneous catalysis and the production of polymer materials.

Sebastian D. Pike

Sebastian D. Pike completed his D.Phil. at the University of Oxford in 2014 under the supervision of Prof. Andrew Weller. Following this, he spent two years working as a post-doctoral research associate in the field of nanoparticle synthesis and catalysis at Imperial College London in the research groups of Prof. Charlotte Williams and Prof. Milo Shaffer. In 2016 he was awarded a Herchel-Smith Research Fellowship at the University of Cambridge. Current research in the Pike group investigates metal-oxide cluster molecules, bridging the fields of molecular and nanoparticle chemistry.

electronics.[6] Nanoparticulate versions of metal oxides retain many of the useful material properties whilst greatly increasing the available surface area, leading to enhanced activity in applications such as catalysis,[7] antibacterial surfaces[8, 9] and sensing.[10, 11] The conductivity of metal oxides may vary from metallic through semiconducting to fully insulating, determined by the electronic band structure of the material. The properties of these materials can be altered upon shrinking the crystallite dimensions into the nanoscale, and even further down to the realm of molecules. In a process known as quantum confinement, the band gap of metal oxides becomes enlarged upon shrinking.[12] Molecular metal-oxo clusters[13] may retain some properties of the related bulk metal oxide, yet typically exhibit enlarged band gaps,[14] they have been applied as light harvesters for photocatalysis;[15] and as single source precursors for chemical vapour deposition techniques.[16] The cluster structures may be recognised as vertices within metal-organic-frameworks (MOFs),[17] and indeed pre-formed metal-oxo clusters may be assembled into microporous MOFs by mechanochemical techniques. Such simple processes promise access to MOFs using rapid, reliable and environmentally friendly synthetic routes.[18-20]

Mixed-metal oxides, such as perovskites and spinels, play an increasingly important role in applications and devices, and have a range of important properties such as superconductance, magnetism and the ability to absorb solar energy.[21, 22] Purposefully doping a secondary metal into a metal oxide has also been shown to influence the optoelectronic properties.[23] At the molecular level, building mixed-metal oxides (with M–O–M' connectivity) enables electronic communication between different metals through bridging oxygen centres, leading to complexes with highly tuneable function. Not only do these mixed-metal-oxo species show promise as effective precursors to mixed/doped metal oxide materials,[24] they also display high catalytic activities within olefin polymerisation[25] and the hydroamination of imines.[26]

Metal oxides are traditionally formed by pH-controlled precipitation from aqueous solutions of metal salts, and the use of ligands or surfactants can help direct the reaction to well-defined nanomaterials. Using a reactive metal precursor that undergoes stoichiometric hydrolysis with water instead, allows improved control over the reaction progress. Stoichiometric reactivity also allows access to partially hydrolysed species, which are inaccessible from aqueous routes. The ability to acquire partially hydrolysed species has played a vital role in

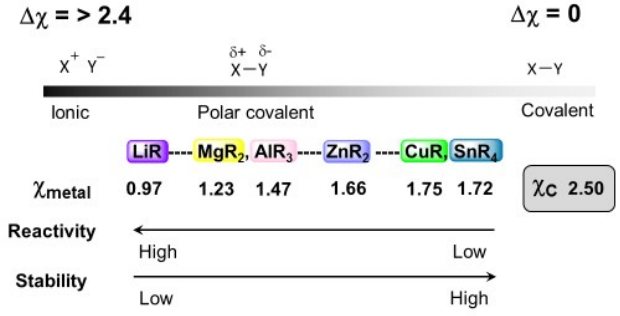

Fig. 1 Scale of organometallic reagents and their properties.

Ziegler-Natta polymerisation chemistry with the discovery of the co-catalyst methylaluminoxane (MAO), formed from $AlMe_3$.[27] A wide range of reactive organometallic and metal-amide reagents are available, which present an emerging class of precursors for the synthesis of metal-oxo clusters, molecular mixed metal-oxo species, and NPs.

1.ii Organometallic and metal-amide reagents: synthesis and structure

Organometallic reagents have revolutionised many research areas, including catalysis, polymerisation chemistry and total synthesis. Their popularity is due to their high reactivity, coupled with their relatively straightforward synthesis and the broad variety of commercially available reagents. Desirable reactivity can often be achieved through careful consideration of the nature of the metal and the organo group, where a greater difference in electronegativity generally gives a more polarised, and hence, more reactive metal–C bond (Fig. 1).[28] The reactivity can often be tuned further through the formation of adducts, such as the addition of a Lewis donor,[29] LiCl salt,[30] or a second, different metal, which can modulate the aggregation state and the charge distribution.[31] Counterbalancing their beneficially high reactivity, organometallic reagents are often pyrophoric, air- and moisture-sensitive, and in some cases, light-sensitive.[32] The Lewis acidic metal centres can interact with water and oxygen, while the unstable and reactive $R^{\delta-}$ group can rapidly react with protic sources such as water.

Most organometallic or metal-amide reagents are derived from highly reactive organolithium, organomagnesium or organoaluminium compounds. The common preparative route for organolithium and organomagnesium reagents is oxidative addition, where the metal is directly added to an organohalide (Fig. 2). This versatile synthetic method is generally well-controlled, although side-reactions such as Wurtz coupling, β-hydride elimination, and the formation of mixed aggregates are possible. Organoaluminium reagents (AlR_3) are often prepared through transmetallation (Fig. 2), with the exchange of an electropositive metal (Al) for a more electronegative metal (Hg), through oxidation of Al by HgR_2. Less reactive organometallic reagents are typically prepared through subsequent metathesis reactions, such as the production of organozinc compounds (ZnR_2) from LiR and $ZnCl_2$, driven by the thermodynamically favourable formation of LiCl. The steric and electronic stabilising effects of the organo group significantly influence the reactivity, and the desired organo group is typically obtained through deprotonative metallation of a more acidic organic substrate such as an amine to form a metal-amide reagent (Fig. 2). These preparative routes are often combined to synthesise a desired reagent, giving access to a multitude of organometallic precursors.

Although M–R bond polarity is key, reactivity is also influenced by the structure and bonding, which is affected by the solvent and the nature of the organo group. Some of the most reactive organometallic precursors display electron deficient bonding, with organo groups bridging between two or

View Article Online
DOI: 10.1039/C8DT00015D

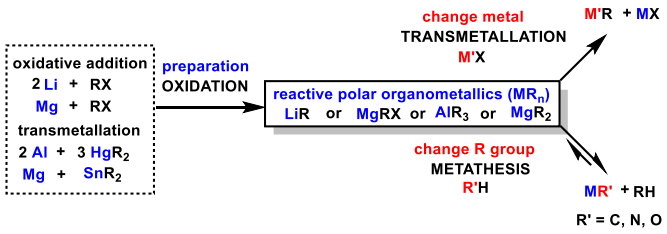

Fig. 2 Synthetic routes to organometallic reagents.

more metal centres. Organoaluminium reagents not only contain electron deficient Al–R–Al (3c-2e) bonds (which are highly polarised and reactive), but also possess low-lying vacant orbitals; these features increase their moisture sensitivity through facilitating nucleophilic attack by water. While still pyrophoric, organozinc reagents display lower reactivities, as lower polarity Zn–C bonds possess a greater covalent character. In the case of dialkyl- or diamide zinc reagents, including $ZnEt_2$[33] and $Zn(N(SiMe_3)_2)_2$,[34] monomeric, linear compounds are formed, which contain 2c-2e Zn–C/N bonds. In contrast, tetra-organotin complexes such as $SnMe_4$ are tetrahedral, electron-precise structures that are not moisture sensitive.[35] While Sn(IV) is the more stable oxidation state, a range of more reactive Sn(II) organometallic and metal-amide complexes are also known.

In contrast to s-block organometallics, transition metal organometallics display an increase in the M–C bond covalency and strength down a triad,[36] arising from the involvement of d-orbitals in the M–C bonding - thus third row organometallics are typically less reactive than their first and second row analogues. The hydrolysis of high oxidation state organometallics such as Cp^*MMe_4 (M = Mo, W) may favour formation of terminal oxo groups (M=O), as such arrangements can help stabilise the high charge upon the metal. For example, Cp^*WMe_4 hydrolyses at elevated temperatures (>65°C) to form methylene bridged $[Cp^*W(=O)(\mu_2\text{-}CH_2)]_2$.[37] In contrast, Cp^*TiMe_3, with a lower oxidation state, reacts to form oxo-bridged dimeric $(Cp^*TiMe_2)_2(\mu_2\text{-}O)$ and trimeric $[Cp^*TiMe(\mu_2\text{-}O)]_3$.[38] Moving across the periodic table towards transition metals of higher electronegativities results in less polarised and less reactive M–C bonds. Whilst copper-alkyl reagents are generally unstable, copper-aryl complexes typically exist as aggregates of Cu_4, Cu_5, Cu_6 or Cu_8.[32] One commonly used precursor, copper mesityl (CuMes, Mes = 2,4,6-$C_6Me_3H_2$), forms structures of different aggregation states depending on the donor solvent, with structural data reported for tetrameric and pentameric ring structures.[39]

While the range of commercially available metal-amides is limited in comparison to organometallic reagents, a growing number may now be purchased, such as $Sn(N(SiMe_3)_2)_2$, $Fe(N(SiMe_3)_2)_2$ and $Zn(TMP)_2$ (TMP = 2,2,6,6-tetramethylpiperidide). Polar metal-amides can be readily prepared through deprotonative metalation of an amine, such as $HN(SiMe_3)_2$ (hexamethyldisilazane), TMP(H) or diisopropylamine, by reaction with organolithium, magnesium, aluminium or zinc reagents. Alternatively, the transmetallation of group 2 metals with Sn(II)-amide reagents is a useful strategy to prepare alkaline-earth metal amides such as $Mg[N(SiMe_3)_2]_2$ (Fig. 2).[41, 42] These polar and reactive metal-amides can be converted to a broad range of lower polarity metal-amides through transmetallation with the relevant metal halide salt.[40]

Although metal-alkoxides $[M(OR)_x]$ are commonly used as precursors to metal oxides,[43] it should be noted that certain examples are not readily accessible: for example zinc [and other M(II)] alkoxides tend to form rather insoluble powders and copper(I) alkoxides are typically unstable. In both these cases commercially available and soluble organometallic reagents (e.g. $ZnEt_2$ and CuMes) are more suitable precursors. Furthermore, the structure, bonding, and hydrolysis pathways of some organometallic reagents are well-established.[44-48] This understanding, in combination with the wide variety that are commercially available or synthetically accessible, gives these reagents great scope as precursors to a range of metal-oxo species.

1.iii Reactivity trends for the hydrolysis of organometallic precursors

Hydrocarbons and amines have much larger pK_a values than water [pK_a values (in water): H_2O, 15.75; NH_3, 37.8; Ph-H, 43.0; Me-H, 48],[49] therefore polar organometallic and metal-amide precursors typically act as strong Brønsted bases and are readily hydrolysed. Brønsted acid/base reactions are typically rapid and exothermic, and can occur at low temperatures. While the hydrolysis of metal-amides is less thermodynamically favourable than the analogous metal-alkyl/aryl reagents, metal-amides can display enhanced kinetic basicity.[50] Studies have suggested that the lone pair of electrons on the NR_2 unit may accelerate the rate of hydrolysis, through facilitating proton transfer from H_2O to the NR_2 unit, to form a hydroxide species.[51, 52] Once formed, M–OH units may undergo subsequent condensation to form M–O–M bonds, within metal-oxo clusters[53] or molecular (mixed-)metal-oxo compounds.[25] In contrast, alcohols have lower pK_a values which are closer to that of water, thus metal-alkoxides generally display poorer Brønsted basicity [pK_a values (in water): MeOH, 15.21; EtOH, 15.85; ^{i}PrOH, 16.48; ^{t}BuOH, 16.54].[54] Despite this lower basicity, the hydrolysis of metal-alkoxides may be driven by an entropically favoured condensation process.

Reactivity trends for the hydrolysis of organometallic reagents typically follow the polarizability of the M–C bond, with the most rapid hydrolysis occurring for the most electropositive metals. The mechanism is generally expected to proceed via nucleophilic attack of water, followed by hydrolysis to a hydroxide intermediate, and subsequent condensation.[44, 55] The nucleophilic attack of water is facilitated by the presence of low-energy vacant orbitals which promote Lewis basic coordination of water to the metal, enabling low activation energy hydrolytic mechanisms via the enhanced acidity of the metal-aqua adduct. Polar organometallics such as MgR_2, ZnR_2, AlR_3 and GaR_3 are readily hydrolysed, thanks to the presence of both highly polarised M–C bonds and low-energy vacant orbitals. Less Brønsted basic organometallic complexes do not deprotonate water as readily: for example, Cp_2TiMe_2 is

View Article Online DOI: 10.1039/C8DT00017C

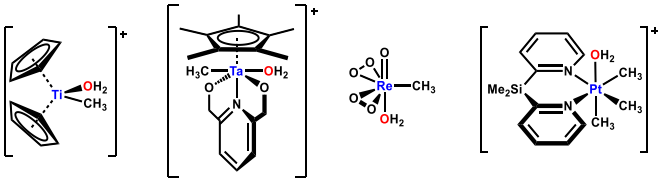

Fig. 3 Examples of organometallic complexes characterised with a metal-alkyl bond and a coordinated water ligand.

reportedly water-stable. Furthermore, the solvent separated aqua complex $[Cp_2Ti(Me)(H_2O)]^+[B(C_6F_5)_4]^-$ synthesized at 205 K (Fig. 3), has been isolated and characterised, a rare example of a first-row transition metal organometallic complex containing both a methyl ligand and a co-ordinated water molecule.[56] The aqua complex, $[Cp_2TiMe(H_2O)]^+$, eventually decomposes by proton transfer from the coordinated H_2O to Me as demonstrated by isotope studies, indicating that an intramolecular proton transfer is key to hydrolysis in this system.[56] Other organo-transition metal aqua complexes bearing more covalent, noble or metastable transition metal–C bonds have also been reported, including $[Cp^*TaMe(\kappa_{N,O,O}2,6\text{-}(CH_2O)NC_5H_3)(H_2O)]^+$,[57] $[Re(Me)(O)(O_2)_2(H_2O)\cdot(diglyme)]$,[58] and various Pt complexes including $(2\text{-pyridyl}_2SiMe_2)PtMe_3(H_2O)$ (Fig. 3).[59]

Within partially hydrolysed metal-oxo species,[13] any unhydrolyzed organo- functionalities (and more strongly bound ligands, such as acac/carboxylate) will act as a ligating shell. The terminology associated with such partially hydrolysed species varies: 'clusters' is a generic term traditionally associated with rigidly coordinated metal-metal bonding, 'poly-oxo-metallate' is commonly attached to charged systems, 'molecular cages' are polycyclic compounds with an internal volume,[60] and sol-gel chemists refer to metal-oxoalkoxides as 'micelles templated by self-assembly of ligands' or 'MTSALs'. More recently, the term 'cluster' (or 'coordination cluster') has also been used for compounds where several metal atoms are connected through bridging atoms or ligands,[61] and so we shall hereafter refer to such species simply as 'metal-oxo clusters'.

To generate M–O–M bonds from organometallic or metal-amide reagents, addition of an oxygen source such as water or M–OH is required, giving good stoichiometric control. In contrast, metal-alkoxide precursors can indirectly generate an oxygen source by reaction or decomposition of the alkoxide ligands. For example, reaction of M–OR with a carboxylic acid can generate an ester and a M–OH unit, whilst the direct formation of M–O–M bonds via release of an ether (R–O–R) has also been suggested at high temperatures.[53, 62] Likewise, the decomposition of $AlR_2(OR)$ or $AlR_2(O_2CR)$ complexes, in the presence of excess AlR_x, may also form Al–O–Al bonds directly alongside alkane or ester byproducts.[63, 64] The reaction of metal-alkoxides with water can thus form mixtures of heteroleptic species bearing hydroxide, alkoxide and/or oxo ligands, and so these processes are often poorly controlled with respect to the stoichiometric incorporation of oxygen.

This article will focus on the hydrolysis of highly reactive MR_x and $M(NR_2)_x$ reagents with water or M–OH units at low temperatures. Advantages of this route include excellent stoichiometric control with the opportunity to isolate and characterise partially hydrolysed intermediates, rapid low temperature reactivity and optional stoichiometric utility of $H_2{}^{17}O$ for NMR studies.[65, 66] Upon hydrolysis, metal-amide reagents form amines that may remain coordinated to the metal as a neutral Lewis basic ligand, although volatile amines such as NMe_2H can be removed *in vacuo*.[67] The hydrolysis of organometallic species can offer an additional benefit, as the alkane or arene by-products are essentially inert and have a negligible effect upon the surface chemistry of the resultant metal-oxo nanostructures. This contrasts with the synthesis of metal-oxo species from the reaction of metal halides with water or alcohols, where the halide may be incorporated into the reaction product.[68, 69]

2. Synthesis of molecular metal-oxo clusters

2.i Hydrolysis of organometallic and metal-amido precursors

The hydrolysis of organometallic and metal-amido precursors can lead to a range of intriguing and useful metal-oxo clusters. This section will explore the formation of homometallic molecular clusters, with a particular focus on well-studied main group organometallics (e.g. AlR_3, GaR_3, ZnR_2). Complexes with bulky and/or chelating ligands which coordinate through M–C or M–N bonds, such as Cp ($[C_5H_5]^-$) and NacNac ($[(N(R)CR')_2CH]^-$), will be discussed in following sections, as these M–ligand bonds are typically more stable to hydrolysis than other M–C/N bonds due to aromaticity and/or resonance stabilisation.

The hydrolysis of trialkylaluminium complexes has been of great interest due to the use of partially hydrolysed MAO as an activator in ethylene and propylene polymerisation reactions since the 1960s.[27] The hydrolysis pathway of AlR_3 reagents have been studied in detail by a combination of *in-situ* NMR spectroscopic studies and the structural characterisation of isolated complexes.[44, 70] Initially, a water molecule binds to form a Lewis adduct, $AlR_3{\cdot}H_2O$, which has been structurally characterised in $Al(C_6F_5)_3(H_2O)$, and the related Ga complex, $Ga(Mes)_3(H_2O)$ (Fig. 4a).[55, 71] While $Ga(Mes)_3(H_2O)$ is stable below 0°C, the Al analogue $Al(Mes)_3(H_2O)$, which exhibits more acidic protons, eliminates MesH at −10°C to form the bridging hydroxide dimer $[Al(Mes)_2(\mu_2\text{-}OH)]_2{\cdot}2THF$.[55] For $Al(C_6F_5)_3(H_2O)$ a strong Lewis adduct interaction, hydrogen bonding contributions, and the reduced Brønsted basicity expected for a fluorinated aryl group stabilise the initial aqua complex, and thus only slow elimination of C_6F_5H occurs at room temperature.[71] Hydroxide species such as $[Al(^tBu)_2(\mu_2\text{-}OH)]_n$ (n = 2,3) have been characterised during hydrolysis of AlR_3 reagents (Fig. 4a).[72, 73] In fact, elevated temperatures are sometimes required to drive the condensation reactions of $[AlR_2(OH)]_n$ species with bulky R groups.[70, 72-74] Condensation often leads to complexes of the form $[AlR(\mu_3\text{-}O)]_n$ (n = 6-12) with cage like structures comprised of Al_3O_3 and Al_2O_2 building units (Fig. 4a).[72, 73] Several species are often simultaneously formed, suggesting equilibrium processes may be occurring. Due to facile redistribution processes, the condensation products formed depend on the reaction medium and temperature.[44]

View Article Online
DOI: 10.1039/C8DT00017D

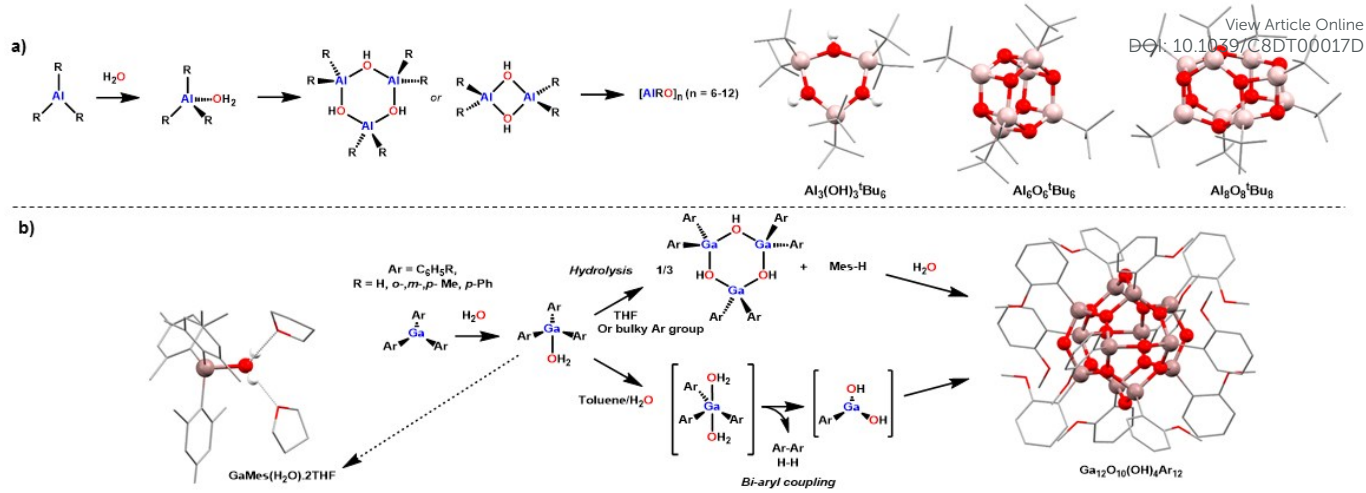

Fig. 4 a) Hydrolysis pathway of AlR_3 precursors. X-ray structures for $Al_3(OH)_3{}^tBu_6$,[72] $Al_6O_6{}^tBu_6$,[72] and $Al_8O_8{}^tBu_8$.[73] b) $GaAr_3$ hydrolysis pathways. Crystal structures for $GaMes_3(OH_2)\cdot 2THF$[55] and $Ga_{12}O_{10}(OH)_4(o\text{-}C_6H_4OMe)_{12}$.[75] Colours: O, red; Al, pale pink; Ga, dark pink.

Reaction with additional water may lead to the formation of hydroxy complexes with persistent Al−R groups (e.g. $[Al_6{}^tBu_6(\mu_3\text{-}O)_4(\mu_2\text{-}OH)_4]$),[76] or alumina gels $[AlO(OH)]_n$.[73] Heavier group 13 Ga and In organometallics form hydroxide complexes readily, but condensation typically becomes slower and requires higher temperatures.[77-79] These metals bear higher electronegativities than Al, which reduces the Brønsted basic nature of the R groups and their susceptibility to hydrolysis. Raston and Atwood studied the hydrolysis of $GaAr_3$ complexes (Ar = C_6H_5R, R = H, *o*-,*m*-,*p*-Me, *p*-Ph) and discovered that the formation of the icosahedral cluster $[Ga_{12}Ar_{12}O_{10}(OH)_4]$ ultimately occurs in the presence of excess water. However, the reaction mechanism is dependent on the solvent medium.[75, 80] In THF, a hydrolysis route occurs via $[GaAr_2(OH)]_3$ with Ar−H released, whereas in a biphasic toluene/water medium intramolecular bi-aryl coupling occurs instead, generating an Ar−Ar by-product and the same icosahedral galloxane cluster [Fig. 4b].[80] The bi-aryl coupling reaction generates H_2 and occurs in the absence of O_2, requiring water to act as the oxidant. The authors propose initial coordination of two water molecules, to form $GaAr_3\cdot 2(H_2O)$, followed by H_2 release and bi-aryl coupling to give $GaAr(OH)_2$, which can oligomerise into $[Ga_{12}Ar_{12}O_{10}(OH)_4]$. Competition experiments showed that when THF was >30% of the organic solvent then the hydrolysis route was favoured, indicating the important role of the coordinating solvent within the hydrolysis mechanism, potentially blocking coordination of a second water to form the $GaAr_3\cdot 2(H_2O)$ intermediate. Such divergent reactivity was not observed for the reaction of $Ga(Mes)_3$ with excess water, which only hydrolyses to generate MesH and the smaller galloxane $[Ga_6Mes_6(\mu_3\text{-}O)_4(\mu_2\text{-}OH)_4]$ in either THF or toluene. It is noteworthy that the initial adduct $GaMes_3\cdot(H_2O)$ could be isolated and structurally characterised (Fig. 4b), perhaps suggesting that the bi-adduct of water, and proposed precursor to bi-aryl coupling, $GaAr_3\cdot 2(H_2O)$, is not accessible in this case. It therefore seems plausible that the enlarged sterics of the mesityl group hinders a bi-aryl coupling pathway.[55]

Studies of the reaction of $ZnEt_2$ with water have also shown the formation of a hydroxide intermediate, $[ZnEt(OH)]_n$ which is likely to exist as a tetramer similar to known $[ZnR(OR)]_4$ complexes.[81] Subsequent elimination of ethane occurs rapidly and allows formation of ZnO (*vide infra*). Hydrolysis of bulkier Zn^tBu_2 allows isolation and structural characterisation of the metastable hexamer $[Zn^tBu(OH)]_6$ (see Fig. 22b, section 4).[82, 83]

Outside of these well studied Al, Ga and Zn systems, the reaction of other MR_x organometallics with water is less studied. One noteworthy set of examples are the reactions of $Sn(R)(CCMe)_3$ with water. Despite the general stability of Sn−R bonds to water, the Sn−alkynyl bonds undergo hydrolysis to produce oxo-clusters such as $[Sn_{12}R_{12}(\mu_3\text{-}O)_{14}(\mu_2\text{-}OH)_6](OH)_2$, $[Sn_{12}(Ar)_8(\mu_4\text{-}O)_2(\mu_3\text{-}O)_8(\mu_2\text{-}O)_4(\mu_2\text{-}OH)_8(OH)_4]$, or a curious hexameric cluster, $[Sn_6(Ar)_6(\mu_3\text{-}O)_4(\mu_2\text{-}O)_2(\mu_2\text{-}OH)_2(OH)_4]$, which can be described as a double-twist Möbius band of stannoxane units (Fig. 5a).[84, 85]

Studies of the hydrolysis of organo-transition metal complexes are uncommon; however, isolated examples of reactions of complexes containing metal−carbon multiple bonds have been reported, for example, the reactions of $W(\equiv E^tBu)(CH_2{}^tBu)_3$ (E = C, Si) and $Mo(=CH^tBu)(CH_2{}^tBu)_2(\equiv N^tBu)$, with excess water.[86-89] In such examples, partial hydrolysis occurs with enhanced reactivity at the M−C/N multiple bonds. The products retain some single M−C bonds highlighting the relative stability of M−C bonds in heavier transition metal complexes, where significant covalency is present.

Hydrolysis of metal-amido complexes also forms M−O−M bonds and can generate metal-oxo clusters, however, reported examples are rare. The group 5 reagents $M(NMe_2)_5$ (M = Nb/Ta) are shown to dideprotonate one equivalent of water to form $[M(NMe_2)_3O]_4$ (Fig. 5b),[90] although further hydrolysis yields insoluble powders. Bergman, Arnold and co-workers also showed the reaction of either $Ta(NMe_2)_5$ or $TaBn_3(=N^tBu)$ with $ArNH_2$ and 1/6 equiv. of water led to the formation of a series of $Ta_6O(=NAr)_{14}$ clusters, indicating a stoichiometric hydrolysis route with either organometallic or metal-amide precursors.[91] Considering the wide range of known metal-amide complexes (especially the $M(N(SiMe_3)_2)_x$ family) there appear to be plenty of unexplored opportunities for forming new metal-oxo clusters by hydrolysis routes, with the benefit that the products may be

View Article Online
DOI: 10.1039/C8DT00017D

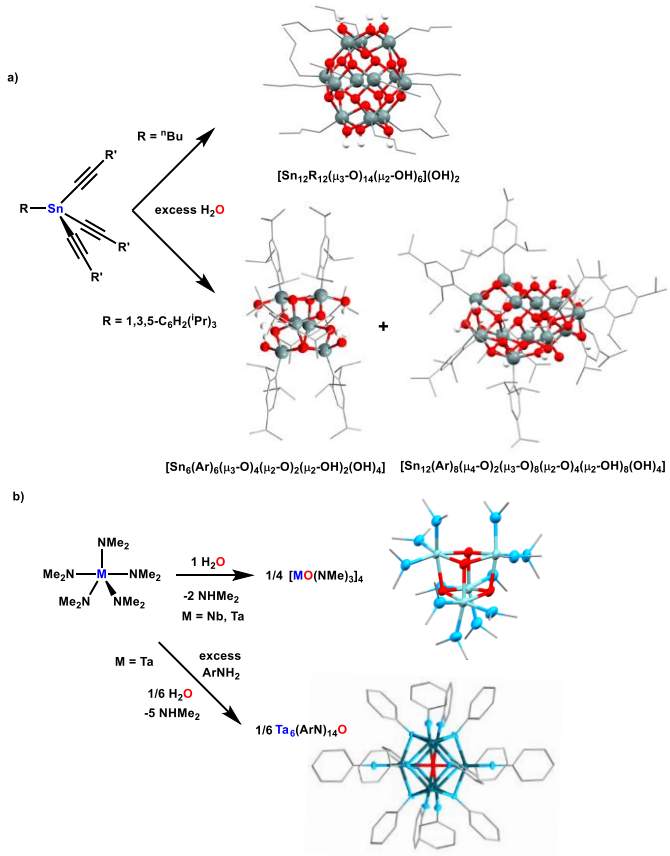

Fig. 5 a) Hydrolysis of alkynyl tin precursors with structures of products; $[Sn_{12}R_{12}(\mu_3\text{-}O)_{14}(\mu_2\text{-}OH)_6]^{2+}$ (anions omitted),[92] $[Sn_{12}(2,4,6\text{-}C_6H_2{}^iPr_3)_8(\mu_4\text{-}O)_2(\mu_3\text{-}O)_8(\mu_2\text{-}O)_4(\mu_2\text{-}OH)_8(OH)_4]$,[84] $[Sn_6(2,4,6\text{-}C_6H_2{}^iPr_3)_6(\mu_3\text{-}O)_4(\mu_2\text{-}O)_2(\mu_2\text{-}OH)_2(OH)_4]$[84] b) Formation of M_4O_4 and M_6O clusters from group 5 metal amido precursors, crystal structures of $[NbO(NMe_2)_3]_4$ and $Ta_6(PhN)_{14}O$.[90,91] Colours: O, red; Sn, grey; N, light blue; Nb, pale turquoise; Ta, teal.

of interest with respect to N-doped metal oxides.[93]

The partial hydrolysis of related metal alkoxides has been studied in detail and is comprehensively reviewed elsewhere.[94] In many cases condensation occurs at elevated temperatures in the absence of added water, suggesting that metal oxy/alkoxy clusters can form through decomposition routes. Metal alkoxide precursors often form a variety of species. For example, complexes exhibiting lower degrees of condensation (e.g. $Ti_3O(OR)_{10}$) are unstable and can react to form more condensed species (e.g. $Ti_{11}O_{13}(O^iPr)_{18}$), with concomitant release of parent $Ti(OR)_4$ precursors through an equilibrium arrangement.[95]

2.ii Hydrolysis of ligated reactive precursors

Organometallic (or metal-amide) precursors may be adapted by adding ligating species; chelating ligands such as carboxylates or dialkylphosphinates $[R_2PO_2]^-$ are often used. The corresponding acid proligands react directly with the Brønsted basic organometallic precursor and bind to the metal. Such ligated metal precursors are expected to retain their coordination to ligands upon initial hydrolysis, which enables extra stabilisation and conformational control, and can also improve solubility properties. Most reported examples of the hydrolysis of ligated organometallics are found for Zn systems. While chelating ligands bind strongly to metal sites, rearrangement and exchange can occur during hydrolysis and in the resulting metal-oxo cluster products, allowing equilibrium conditions to selectively form thermodynamically favoured structures.[96] Such ligand mobility is also regularly reported for ligated metal-oxo-alkoxide structures.[53, 97-99] The ability to direct reactions through well-defined intermediates is a key consideration in the growth of extended metal-oxide nanostructures from molecular precursors. However, due to equilibration and rearrangement, the products of each hydrolysis step bear little structural resemblance to their precursors.[100] The introduction of bridging oxo ligands directs self-assembly of condensed units, such as M_4O tetrahedra, and may initiate the rearrangement (or even loss) of ligands in the precursor. Therefore, in most cases, the eventual assemblies should not be influenced by the molecular precursor design. Nonetheless, the quantity of strongly binding ligands can influence the growth of condensation products, either supporting small clusters or allowing growth of extended metal-oxide domains. If the precursors have a high ligand content then hydrolysis is likely to lead to small ligated metal-oxo-clusters, such as tetrahedral Zn_4OL_6 (L = carboxylate, carbamate, amidate, phosphinate or dialkylphosphate),[18, 96, 101-103] formed through the straightforward stoichiometric hydrolysis of a 2:3 ratio of $ZnEt_2$ and ligand. This tetrahedral unit has been commonly used as a vertex within MOFs and pre-assembled $Zn_4O(amidate)_6$ clusters act as a precursor to the mechanochemical formation of MOF-5.[17, 18] Bury, Lewiński and co-workers reported that introducing additional water to $Zn_4O(PhCO_2)_6$ in THF resulted in the formation of adduct $Zn_4O(PhCO_2)_6(H_2O)(THF)\cdot 2THF$, where one zinc centre changes from a tetrahedral coordination environment to a pseudo-octahedral one (Fig. 6).[104] Such findings have implications for the stability and reactivity of MOFs in the presence of moisture. Intriguingly the reactivity of $Zn_4O(Ph_2PO_2)_6$ displays a very different onward reaction with water: in hydrophobic solvents such as $CDCl_3$ or d_8-toluene the original Zn_4 cluster exhibits an equilibrium relationship with an extended zinc-hydroxy cluster, $Zn_6(OH)_3(Ph_2PO_2)_6$ (Fig. 6b).[96] It appears that changing the ligand from $[PhCO_2]^-$ to the slightly larger $[Ph_2PO_2]^-$ favours expansion to form a larger cluster, possibly due to a relaxation of bond strain in the chelating phosphinate ligand.

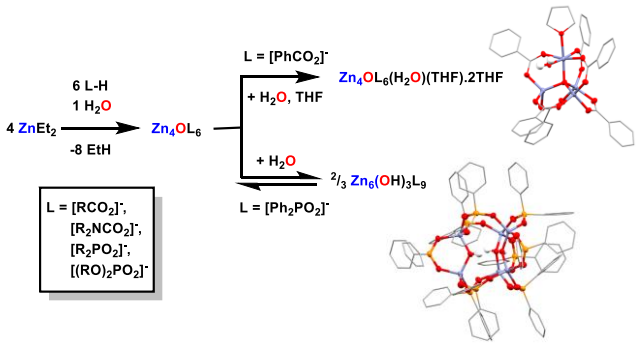

Fig. 6 Synthesis of Zn_4OL_6 clusters from $ZnEt_2$ and reactions with excess water.[96, 101-104] Colours: O, red; Zn, blue; P, orange.

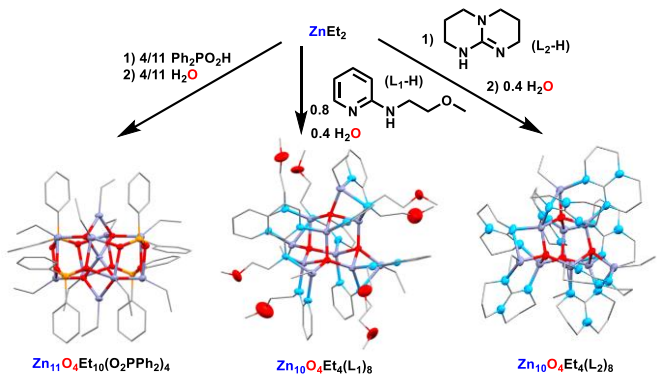

Fig. 7 ZnO clusters formed by partial hydrolysis of $ZnEt_2$ and/or ZnEtL.[96, 105, 106] Colours: O, red; Zn, blue; P, orange; N, light blue

Larger Zn-oxo clusters can be synthesized by using a lower ligand:Zn ratio. For example, $Zn_{11}O_4Et_{10}(Ph_2PO_2)_4$ was synthesized by adding the required stoichiometry of water to a 1:7 mixture of $[ZnEt(Ph_2PO_2)]_4$ and $ZnEt_2$ (Fig. 7).[96] Recently, two ZnO supertetrahedron structures were reported from the partial hydrolysis of either $ZnEt_2$ with ~0.8 equiv 2-$C_6H_4N(NHC_2H_5OMe)$ or from ZnEtL (L = 1,3,4,6,7,8-hexahydro-2*H*-pyrimido[1,2-*a*]pyrimidine).[105, 106] Both complexes have formulae $Zn_{10}Et_4O_4L_8$ with a heteroadamantane $Zn_{10}O_4$ core (Fig. 7). In the first case, the complex is active as a catalyst for ring-opening polymerisation of L-lactide and ε-caprolactone.[106] In the second case, it is unusual that partial hydrolysis of ZnEtL (10 equiv.) with H_2O (4 equiv.) releases Et−H (6 equiv.) and L−H (2 equiv.), rather than exclusively releasing alkane.[105] Steiner and co-workers reported the reaction of $ZnEt_2$ with amino-phosphazenes $(RNH)_6P_3N_3$ (Fig. 8) under dry conditions to form $\{(RN)_3(RNH)_3P_3N_3\}_2(ZnEt)_6$.[107] Employing the well-defined hydrates $(RNH)_6P_3N_3.xH_2O$ instead led to structures with ZnO fragments elegantly sandwiched between two ligands (Fig. 8). Either a planar Zn_3O_3 ring or hexagonal Zn_6O_6 prism could be captured by capping with $\{(RN)_3(RNH)_3P_3N_3\}(ZnEt)_3$ units.[107]

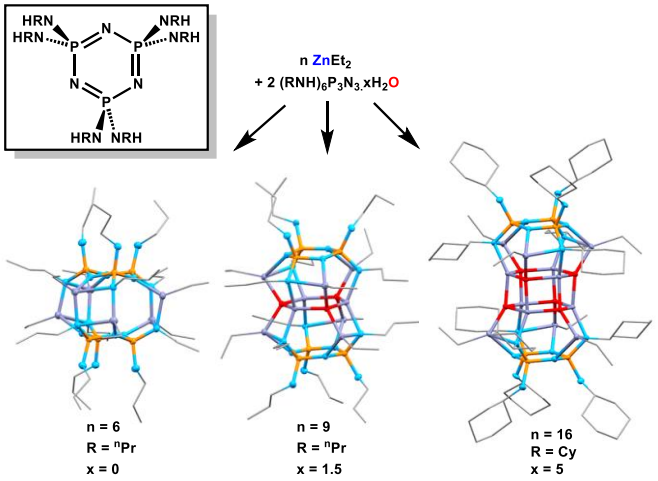

Fig. 8 The reaction of amino-phosphazene (hydrates) with $ZnEt_2$ which can trap ZnO fragments in the reaction products; $\{(^nPrN)_3(^nPrNH)_3P_3N_3\}_2(ZnEt)_6$, $\{(^nPrN)_3(^nPrNH)_3P_3N_3\}_2(ZnEt)_6(ZnO)_3$, $\{(CyN)_3(CyNH)_3P_3N_3\}_2(ZnEt)_6(ZnO)_6$.[107] Colours: O, red; Zn, blue; P, orange; N, light blue

Outside of zinc reagents, the hydrolysis of ligated organometallics to generate metal-oxo clusters is generally restricted to the formation of small dimeric or trimeric, oxygen bridged species. For example, Cp_2MMe_2 (M = Hf, Zr) undergo facile hydrolysis under air, with the formation of linear dimers $[(Cp_2MMe)_2(\mu_2\text{-}O)]$,[108, 109] whilst Cp^*TiMe_3, reacts with water to generate trimer $[Cp^*TiMe(\mu_2\text{-}O)]_3$.[38] Controlled hydrolysis of magnesium complexes such as tris(pyrazolyl)hydroborato (Tp) ligated $[(Tp^{Ar,Me})Mg(Me)\cdot(THF)]$ (Ar = *p*-butyl-C_6H_4) often leads to the formation of dimeric hydroxy complexes, such as $[(Tp^{Ar,Me})Mg(\mu\text{-}OH)]_2$.[110]

The hydrolysis of organometallics and metal-amides shows promise in forming partially hydrolysed metal-oxo clusters. While the introduction of ligands can stabilise the formation of larger structures, divergent reactivity to form ligated clusters and bulk metal-oxides may occur when a small proportion of ligand is used.[96]

3. Metal hydroxyl complexes as protic precursors for oxo-bridged heterometallic motifs

3.i Synthetic routes towards building M–O–M' connectivity

When two different metal centres are connected through a bridging heteroatom within a molecular environment, electronic and chemical communication between the two metals occurs. This connectivity can alter the Lewis acidity of the metal centres, and such heterometallic (mixed-metal) species often display different chemical reactivity compared to the homometallic analogues, leading to new properties such as enhanced catalytic activities.[25, 28] While a broad range of heterometallic systems are known, this section will focus on oxo-bridged systems bearing M–O–M' connectivity. Such complexes have been applied as olefin and ring-opening polymerisation catalysts, and have shown promise as single site precursors for the synthesis of mixed-metal oxide NPs and materials with carefully controlled metal-metal' ratios.[24, 111]

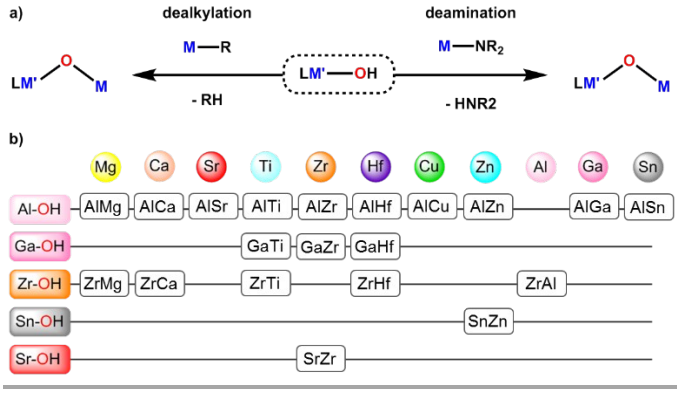

Fig. 9 a) General schematic for the synthesis of molecular mixed-metal-oxo species through dealkylation or deamination routes. b) Known combinations for structurally characterised molecular mixed-metal-oxo (M-O-M') clusters, synthesised through dealkylation or deamination pathways.

The dealkylation or deamination of organometallic or metal-amide reagents, through reaction with metal-hydroxyl compounds, provides a useful strategy to prepare molecular heterometallic oxo species in a controlled manner (Fig. 9). A wide range of well-defined M–OH complexes are known[82, 112] and can be accessed through controlled hydrolysis routes.[44, 110, 113-115] Subsequent deprotonation of the Brønsted acidic -OH proton with a highly Brønsted basic organometallic or metal-amide reagent can generate a range of heterometallic oxo species. The success of these reactions typically depends on the Brønsted acidity of the OH proton; the nucleophilicity of the organometallic or metal-amide reagent; and the careful selection of the supporting ligand. This versatile approach has been applied to a range of main group and transition metals (Fig. 9b). Alternatively, the use of protic non-metallic hydroxides (E–OH) can also hydrolyse organometallic fragments to generate M–O–E structures.[116, 117] For example, $B(OH)_3$ reacts with $ZnEt_2$ (2 equiv.) and Ph_2PO_2H (3 equiv.) to form the cluster $Zn_6(Ph_2PO_2)_9(BO_2)_3$, in which three $B(OH)_3$ units combine to form a central B_3O_3 boroxine ring.[96] While a vast amount of research has focused on the conversion of M–OR groups to M–O–M' units, this topic has been extensively covered in other reviews and will not be discussed in detail here.[118,69] Other successful yet less widely-developed strategies to form oxo-bridged heterometallic complexes include C–H deprotonation to yield zwitterionic complexes;[119, 120] oxidation of heterometallic precursors;[121, 122] use of a heterometallic reagent to encapsulate oxo dianions from air or ethereal solvents;[123-125] or adduct formation from a donor M=O functionality to a Lewis acidic metal centre.[126] Here we shall focus on the well-established and versatile dealkylation or deamination routes from organometallic/metal-amide precursors.

3.ii Building Al-O-M' bridges from Al–OH reagents

While the formation of mixed-metal-oxo species through dealkylation/deamination is a general method, this concept has been best established for aluminium species.[25, 44] Heterometallic complexes based on aluminium are particularly attractive as many are potent ethylene polymerisation catalysts, which blend a single site homogenous catalyst with a well-defined alumoxane unit.[25] A range of Al–O–M complexes have been prepared from ligand supported Al–OH species bearing Brønsted acidic protons, including AlMg,[127] AlCa,[128] AlSr,[128] AlTi,[129] AlZr,[130] AlHf,[28] AlCu,[131] AlZn,[132] AlGa[133] and AlSn[134] systems.

As organometallic complexes with a terminal Al–OH unit are often unstable (refer to Section 2), the preparation of these compounds can be a synthetic challenge. In spite of this, several examples of ligand supported Al–OH precursors are known (Fig. 10), particularly those based on sterically bulky β-diiminate ligand frameworks. Complexes of general formula LAl(R)(OH) are formed from hydrolysis of LAl(R)Cl, in the presence of a N-heterocyclic carbene as a HCl scavenger.[135] In certain cases, Al–OH complexes can be accessed by controlled hydrolysis of a reactive organoaluminium complex, such as the preparation of $[(L_{TBBP})Al(OH).THF]_3$ from $[(L_{TBBP})AlMe{\cdot}THF]$ and water. Unlike

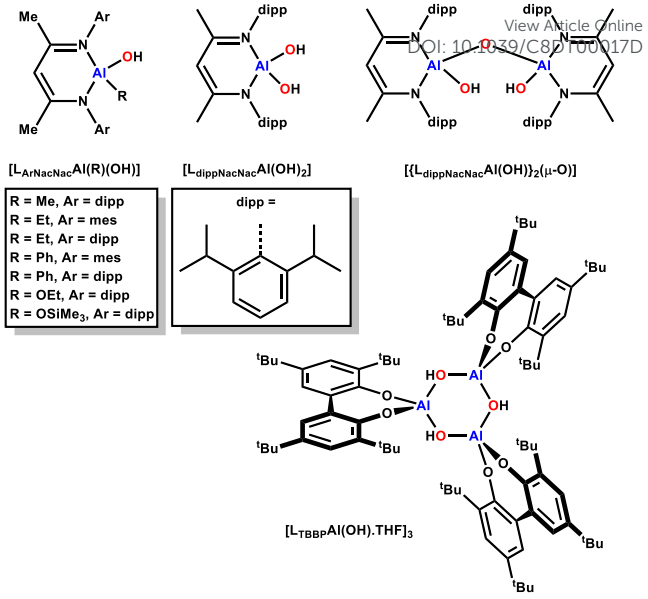

Fig. 10 Ligand supported aluminium hydroxide precursors.[135-139]

the majority of ligand supported Al–OH precursors, $[(L_{TBBP})Al(OH){\cdot}THF]_3$ has a trimeric structure, with a central $\{Al(OH)\}_3$ core (Fig. 10).[137] While it could be expected that OH groups that bridge between two Lewis acidic Al^{3+} centres would display enhanced Brønsted acidity, in practice this is not straightforward. For example, trimeric $[(L_{TBBP})AlOH{\cdot}THF]_3$ does not display sufficient Brønsted acidity to dealkylate $Cp^*_2ZrMe_2$. This lack of reactivity has also been observed with other bridged hydroxide complexes such as $[^{Me}L_{MesNacNac}Zn(OH)]_2$,[132] and may arise from steric protection of the M–OH group. In addition to the bridging or terminal nature of the Al–OH bonds, the aggregation state, steric bulk and electronics of the supporting ligand, and nature of the anionic groups (R, OH or O) can influence the Brønsted acidity of the M–OH unit. The relative ^1H NMR chemical shifts of the M–O*H* protons can give some indication of their acidity, with downfield -OH resonances generally expected to display greater Brønsted acidic character.[144] While such comparisons are somewhat limited by solvent effects and the presence of hydrogen bonding, the chemical shifts can give a useful indication of the influence of the ligand and substituents upon the Brønsted acidity (Table 1). In C_6D_6, the Al–O*H* resonance of complexes based on the BDI-based ligand, *e.g.* $[L_{dippNacNac}Al(R)(OH)]$, shifts upfield (towards weaker Brønsted acidity) in the order R = Me (0.53 ppm), [140] R = OH (0.22 ppm), [141] R = O–Al' (–0.64 ppm)[142] (Fig. 10). While this order is perhaps counterintuitive, as electronegative substituents would generally be expected to enhance the

Table 1 ^1H NMR shifts of BDI-ligand supported metal-O*H* precursors in C_6D_6 solvent.

Compound	^1H NMR shift δ (ppm)	Reference
$[L_{dippNacNac}Al(Me)(OH)]$	0.53	140
$[L_{dippNacNac}Al(OH)_2]$	0.22	141
$[\{L_{dippNacNac}Al(OH)\}_2(\mu\text{-}O)]$	–0.64	142
$[L_{dippNacNac}Ga(Me)(OH)]$	0.08	143
$[\{L_{MesNacNac}Ga(OH)\}_2(\mu\text{-}O)]$	–1.38	43
$[L_{MesNacNac}Zn(OH)]$	–0.20	132

View Article Online
DOI: 10.1039/C8DT00017D

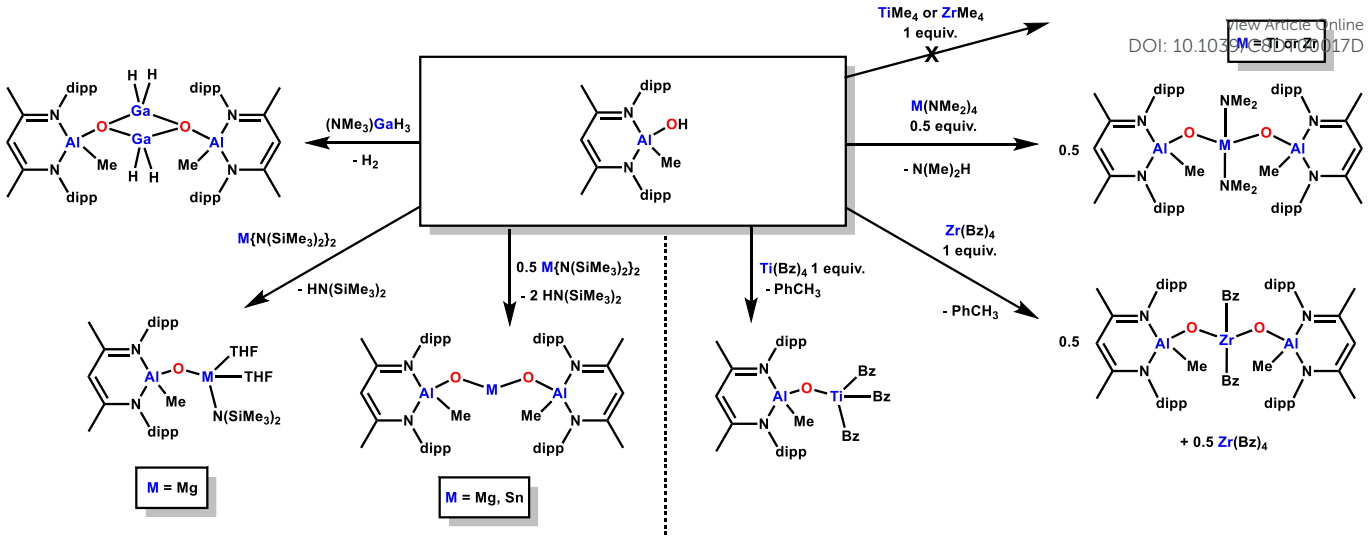

Fig. 11 Reactivity of [$L_{dippNacNac}$Al(Me)(OH)] with various organometallic and metal-amide reagents. Left) Formation of heterometallic main group Al–O–Ga, Al–O–Mg and Al–O–Sn oxo species.[127, 134, 136] Right) Influence of organometallic or metal-amide reagent upon the product formation and M–O–M' stoichiometry.

Brønsted acidity of a substrate, these systems are not straightforward as the –OH is located on a metal centre.[145] These ^{1}H NMR shifts suggest that the Al–OH protons of [$^{Me}L_{dippNacNac}$Al(Me)(OH)] display the greatest Brønsted acidity. This correlates with the chemical shifts (Table 1) and experimentally observed reactivity trends for analogous gallium-hydroxide precursors (*vide infra).*

The deamination of Mg{N(SiMe$_3$)$_2$}$_2$ by aluminium hydroxide [$L_{dippNacNac}$Al(Me)(OH)] has been used to synthesise heterometallic [$L_{dippNacNac}$Al(Me)(μ-O)Mg{N(SiMe$_3$)$_2$}] (Fig. 11).[127] Due to the high Brønsted basicity of both Mg–N(SiMe$_3$)$_2$ units, altering the Mg:Al reaction stoichiometry to 1:2 results in the formation of the trimetallic oxo bridged unit Al–O–Mg–O–Al within [{$L_{dippNacNac}$Al(Me)(μ-O)}$_2$Mg]. This trimetallic complex bears the same metal-metal' ratio as the spinel ($MgAl_2O_4$), and has potential as a useful precursor to bulk mixed-metal oxides. Using sterically unhindered gallium hydride as the base gave dimeric heterometallic complex, [$L_{dippNacNac}$Al(Me)(μ-O)GaH$_2$]$_2$, bearing a [GaO]$_2$ galloxane core (Fig. 11).[136] This –OH deprotonation strategy has also been applied to less Brønsted basic main group reagents, such as Sn{N(SiMe$_3$)$_2$}$_2$ (Fig. 11).[134]

Oxophilic group 4 organometallic and metal-amide reagents have also been used to deprotonate Brønsted acidic [$L_{dippNacNac}$Al(Me)(OH)] (Fig. 11). While this is generally a successful method to access mixed-metal-oxo species, the choice of the metal, nature of the organo- or amide group, and the reaction stoichiometry influences whether a bimetallic (Al–O–M) or trimetallic (Al–O–M–O–Al) core is accessed (M = Ti, Zr, Hf). With benzyl precursor TiBn$_4$, altering the reaction stoichiometry from 1:1 to 2:1 (Al:Ti) allowed the controlled synthesis of bimetallic $L_{dippNacNac}$Al(Me)(μ-O)TiBn$_3$] or trimetallic [{$L_{dippNacNac}$Al(Me)(μ-O)}$_2$TiBn$_2$], respectively. In contrast, using ZrBn$_4$ as the Brønsted base selectively gave trimetallic [{$L_{dippNacNac}$Al(Me)(μ-O)}$_2$ZrBn$_2$], irrespective of the stoichiometry of the starting reagents.[146] While sterically unhindered metal-amides Ti(NMe$_2$)$_4$ and Zr(NMe$_2$)$_4$ can generate trimetallic [{$L_{dippNacNac}$Al(Me)(μ-O)}$_2$M(NMe$_2$)$_2$],[130] the analogous reactions with TiMe$_4$ or ZrMe$_4$ were unsuccessful, resulting in the formation of elemental Ti or Zr.[147] In general, with bulky [$L_{dippNacNac}$Al(Me)(OH)] precursors and tetravalent group 4 reagents, only one or two of the alkyl/amide units will react to generate Al–O–M or Al–O–M–O–Al units, respectively.[147] So far, this synthetic strategy appears to be somewhat limited in its use for preparing complexes with more than three metal centres from a monohydroxide precursor.

The selection of an appropriate ligand is important as it can influence the stability of the heterometallic product. Deprotonation of [$L_{dippNacNac}$Al(Me)(OH)] with Cp$_2$M(Me)$_2$ (M = Ti, Zr or Hf) leads to the formation of [$L_{dippNacNac}$Al(Me)(μ-O)M(Me)Cp$_2$], driven by the accompanying formation of methane gas (Fig. 12).[129, 135, 140] In contrast to reaction with Cp$_2$TiMe$_2$ or CpTiMe$_3$,[148] reaction of [$L_{dippNacNac}$Al(Me)(OH)] with [$L_{dippNacNac}$TiMe$_3$] does not yield a stable heterometallic product. Instead [$L_{dippNacNac}$Al(Me)(μ-O)Ti(Me)$_2$$L_{dippNacNac}$] undergoes slow

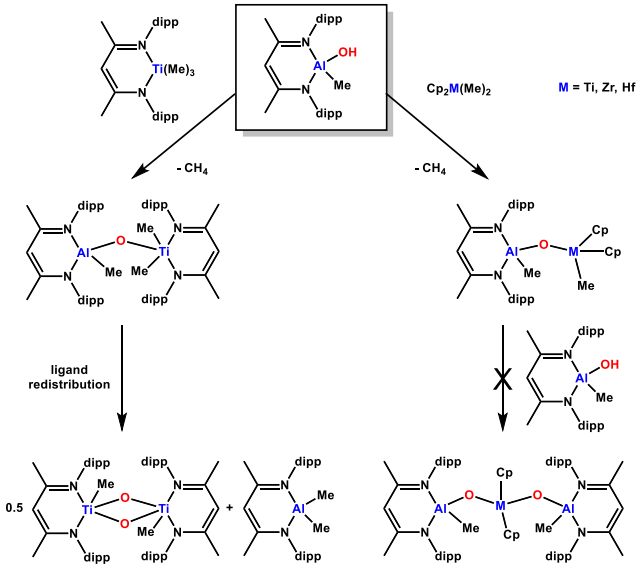

Fig. 12 Ligand influence upon product formation and stability of oxo-bridged heterometallic AlTi complexes. [129, 135, 149]

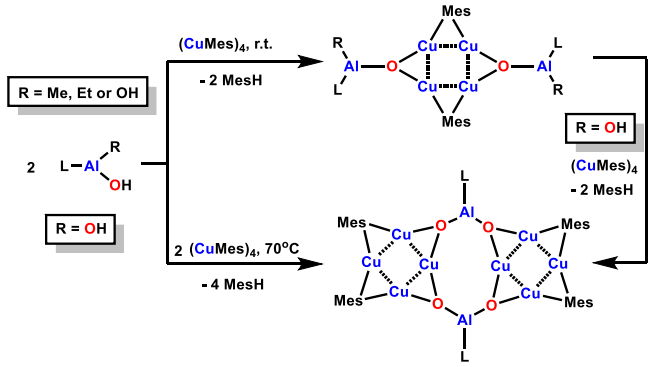

Fig. 13 Synthesis of Cu-O-Al species through dealkylation reactions.[131]

ligand redistribution to form homometallic complexes $[L_{dippNacNac}Ti(Me)O]_2$ and $[L_{dippNacNac}AlMe_2]$ (Fig. 12).[149]

When paired with a strongly Brønsted acidic Al–OH unit, dealkylation of weaker Brønsted bases such as organocopper reagents can be achieved. The reaction of monohydroxide $[L_{dippNacNac}Al(R)(OH]$ with CuMes gave the Al–O–Cu based species $[L_{dippNacNac}Al(R)(\mu_3\text{-}O)Cu_2Mes]_2$ (Fig. 13).[131] When the related dihydroxide species, $[L_{dippNacNac}Al(OH)_2]$, was applied as the precursor and the reaction performed at ambient temperature, $[L_{dippNacNac}Al(OH)(\mu_3\text{-}O)Cu_2Mes]_2$ was formed, with a reactive OH group retained on each Al centre. Performing the reaction at 70°C, or reacting the initial product, $[L_{dippNacNac}Al(OH)(\mu_3\text{-}O)Cu_2Mes]_2$, with a further equivalent of CuMes, yielded the dimeric product $[L_{dippNacNac}Al(\mu_3\text{-}O)_2Cu_4Mes_2]_2$, where two Cu_4 units are bridged by two AlO_2 units (Fig. 13).

Expanding upon Al–OH precursors, alumosiloxanes with a Si–O–Al–OH unit are also accessible. Deprotonation of such precursors has successfully led to the synthesis of novel alumosiloxanes bearing Si–O–Al–O–Ga,[133] Si–O–Al–O–Ti/Zr/Hf,[147] Si–O–Al–O–Zn,[150] or Si–O–Al–O–Sn[151] cores. For example, $[L_{dippNacNac}Al(OH)(\mu_2\text{-}O)Si(OH)(O^tBu)_2]$ was derivatised through reaction with a range of organometallic reagents including $ZnMe_2$ and $GaMe_3$, to generate heterometallic alumosiloxanes (Fig. 14).[133] In all cases, the

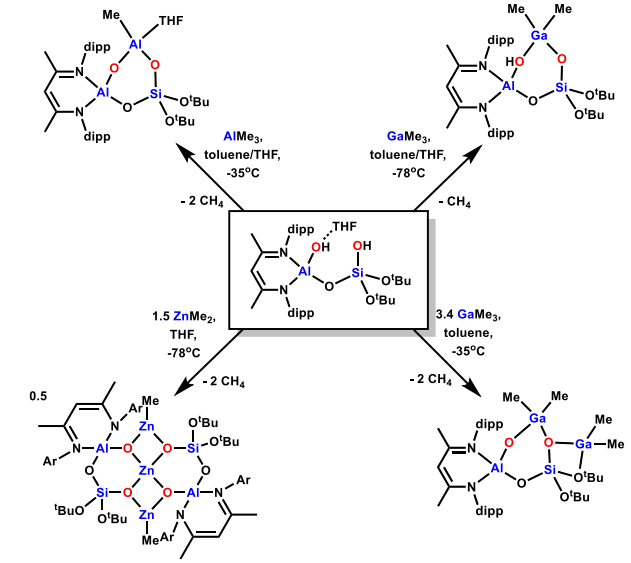

Fig. 14 Synthesis of heterobimetallic alumosiloxane species.[133]

Si–OH proton displayed greater Brønsted acidity than the Al–OH proton, which may be partly due to the steric bulk of the dipp groups providing steric protection for the Al–OH unit. In this competition system, the Si–OH unit was either deprotonated before Al–OH, or was the only OH group to be deprotonated. Thus, the Brønsted basicity and steric bulk of the organometallic or metal-amide reagent becomes highly important. Highlighting the difference in reactivity between $AlMe_3$ and $GaMe_3$, the reaction of $[L_{dippNacNac}Al(OH)(\mu_2\text{-}O)Si(OH)(O^tBu)_2]$ with strongly Brønsted basic $AlMe_3$ (1 equiv.) gave the dideprotonation product, $[L_{dippNacNac}Al(\mu_2\text{-}O)_2Si(O^tBu)_2(\mu_2\text{-}O)Al(Me)]$. In contrast, reaction with $GaMe_3$ (1 equiv.) resulted in monodeprotonation (of only the Si–OH unit), to form $[L_{dippNacNac}Al(OH)Si(O^tBu)_2(\mu\text{-}O)GaMe_2]$. Excess $GaMe_3$ (3.4 equivalents) was required to deprotonate the Al–OH unit (Fig. 14). Dideprotonation was also achieved using Me_2Zn (1.5 equiv.), to generate a heterometallic species bearing a [Al–O–Si–O–Zn–O] core (Fig. 14).[133]

3.iii Deprotonation of Ga–OH reagents to form Ga-O-M' connectivity

Complexes bearing Ga–O–M' connectivity have also been prepared through dealkylation and deamination routes, although fewer examples are known. Common precursors include $[L_{dippNacNac}Ga(Me)OH]$[143] and $[(Mes)_2Ga(\mu\text{-}OH)_2Ga(Mes)_2{\cdot}2THF]$.[146] While $[L_{dippNacNac}Ga(Me)OH]$ was synthesised from a similar method to the aluminium analogue,[143] the dimeric mesityl precursor was prepared by the controlled hydrolysis of trimesitylgallium with water, in THF solvent.[55] Highlighting the weaker Brønsted acidity of Ga–OH units in comparison to Al–OH units, the Ga–O*H* ^{1}H NMR resonances have an upfield chemical shift compared to analogous Al–O*H* resonances (Table 1).[55] For example, $[L_{dippNacNac}Ga(Me)(OH)]$[143] has a Ga–O*H* resonance at 0.08 ppm, whereas the Al–O*H* resonance of $[L_{dippNacNac}Al(Me)(OH)]$ arises at 0.53 ppm (both in C_6D_6 solvent).[140]

The deprotonation of $[L_{dippNacNac}Ga(Me)(OH)]$ with Cp_2ZrMe_2 led to heterometallic $[L_{dippNacNac}Ga(Me)(\mu\text{-}O)Zr(Me)Cp_2]$ in a straightforward manner.[143] In contrast, the deprotonation of $[(Mes)_2Ga(\mu\text{-}OH)_2Ga(Mes)_2{\cdot}2THF]$ by $Ti(NEt_2)_4$ is more complex; using a 1:3 ratio of reagents gave a mixed-metal $[Ga_6Ti]$ oxo cluster (Fig. 15).[146] Interestingly, the solid state structure of this cluster suggests that metathesis has occurred, as the NEt_2 ligands have been transferred from Ti to Ga, and $GaMes_3$ was observed along with mesitylene and $HNEt_2$. Such metathesis reactions have been observed with other gallium-based oxo systems; the reaction of $[L_{dippNacNac}TiMe_3]$ with $[(Mes)_2Ga(\mu\text{-}OH)_2Ga(Mes)_2{\cdot}2THF]$ gave the homometallic oxo-bridged species $[L_{dippNacNac}Ti(Me)(\mu\text{-}O)_2Ti(Me)L_{dippNacNac}]$, along with

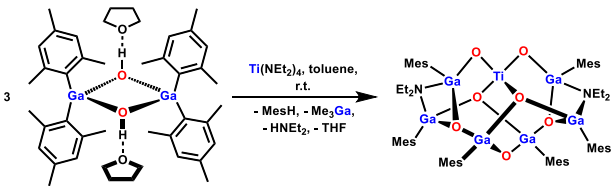

Fig. 15 Synthesis of a mixed-metal GaTi oxo cluster.[146]

View Article Online
DOI: 10.1039/C8DT00017D

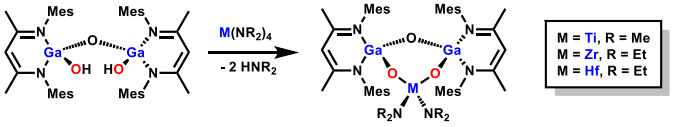

Fig. 16 Synthesis of heterometallic galloxane complexes.[152]

$GaMes_3$.[149] A range of heterometallic galloxane complexes have been prepared from a dihydroxide precursor, [{$L_{MesNacNac}$Ga(OH)}$_2$(μ-O)] (Fig. 16).[152] Dideprotonation by group 4 amide reagents [Ti(NMe$_2$)$_4$, Zr(NEt$_2$)$_4$ or Hf(NEt$_2$)$_4$] led to the synthesis of [{($L_{MesNacNac}$Ga)$_2$(μ-O)}(μ-O)$_2${M(NR$_2$)$_2$}]. It is noteworthy that while the Ga—OH unit deaminates organoamide reagents, no reaction occurred with trialkylaluminium or gallium reagents ($AlMe_3$ or $GaMe_3$), or with Cp_2MMe_2 (M = Ti, Zr or Hf). This lack of dealkylation may arise from the steric bulk of the group 4 organometallic reagents. Alternatively, the reactivity observed with Ti(NMe)$_4$ or Zr/Hf(NEt)$_4$ may be attributed to the enhanced kinetic basicity of organoamide units[50] and the ability of the lone pair of electrons on N to facilitate proton transfer.[51, 52]

Comparison of the ^{1}H NMR spectra of these Ga-O*H* precursors suggests that the galloxane precursor [{$L_{MesNacNac}$Ga(OH)}$_2$(μ-O)] will display weaker Brønsted acidity than [$L_{dippNacNac}$Ga(Me)(OH)], as the Ga-OH ^{1}H NMR resonance is further upfield (−1.38 ppm and 0.08 ppm respectively, both in C_6D_6).[143, 152] The experimental data provides support for these relative Brønsted acidities, as while [$L_{dippNacNac}$Ga(Me)(OH)] dealkylates Cp_2ZrMe_2,[143] the bis-Ga precursor [{$L_{MesNacNac}$Ga(OH)}$_2$(μ-O)] does not.[152] The bis-Ga precursor also displays lesser acidity than the Al analogue [{$L_{dippNacNac}$Al(OH)}$_2$(μ-O)] in line with the -O*H* ^{1}H NMR shifts (Al-O*H*, −0.64 ppm; Ga-O*H*, −1.38 ppm both in C_6D_6)[142] and evidenced by the lack of ability of the Ga species to dealkylate organoaluminium reagents.[139, 152]

3.iv Applying Zr–OH complexes to build Zr-O-M' units

The zirconium precursor [Cp*$_2$Zr(Me)(OH)] can be prepared by hydrolysis of [Cp*$_2$ZrMe$_2$] with one equiv. of water, with concomitant formation of methane gas.[153] The hydroxyl complex is monomeric in the solid state, and displays good stability even at elevated temperatures. The choice of ligand and R group are important for stabilising the hydroxide, as the reaction of either [Cp_2ZrMe_2] or [Cp*$_2$ZrH$_2$] with one equiv. of water leads instead to oxo-bridged dimeric species.[109, 137, 154]
Based on the reaction of [Cp*$_2$Zr(Me)(OH)] with a ligand supported LAlMe complex, Harder and co-workers have developed complexes bearing Zr–O–Al connectivity as efficient olefin polymerisation catalysts [L = L_{TBBP} or L_{DIPH}, L_{DIPH} = 3,3'-bis(2-methylallyl)-(1,1'-biphenyl)-2,2'-diol).[137, 155] From a reactivity perspective, the synthesis of these complexes demonstrates the importance of the nature of the LM–OH and the LM'–R reagents in accessing the desired M–O–M' connectivity. Beginning with the aluminium monohydroxide complex [(L_{TBBP})Al(OH)]$_3$ and [Cp*$_2$ZrMe$_2$] or [Cp_2ZrMe_2], no dealkylation was observed. However, simply swapping the ligand-supported metals of the M–OH and M'–R units, by combining [(L_{TBBP})Al(Me)·THF]$_3$ and [Cp*$_2$Zr(Me)(OH)], the

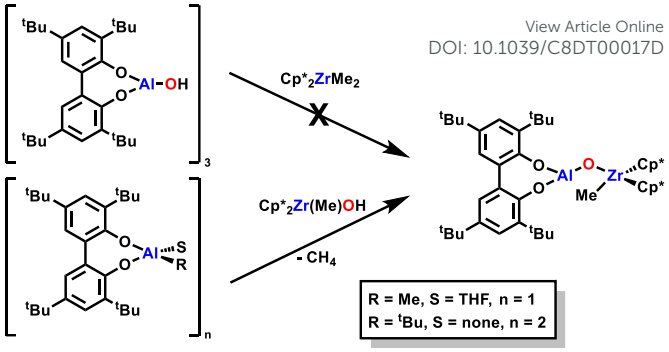

Fig. 17 Synthesis of [(L_{TBBP})Al(μ-O)Zr(Me)Cp*$_2$].[137]

targeted complex [(L_{TBBP})Al(μ-O)Zr(Me)Cp*$_2$] was accessed (Fig. 17).[137] The successful deprotonation of the Zr–OH units may be due to their greater accessibility, as X-ray diffraction studies show that [Cp*$_2$Zr(Me)(OH)] is monomeric with terminal -OH units,[153] in contrast to trimeric [L_{TBBP}Al(OH)·THF]$_3$, which contains bridging -OH units.[137] In general, other aluminium-hydroxide precursors have successfully dealkylated organozirconium reagents, such as the reaction of [$L_{dippNacNac}$Al(Me)(OH)] and [$Cp_2Zr(Me)_2$] to form [$L_{dippNacNac}$Al(Me)(μ-O)Zr(Me)Cp$_2$].[140]

Precursor [Cp*$_2$Zr(Me)(OH)] has proven to be a generally effective Brønsted acid,[156] and has been applied to the dealkylation of [Cp*TiMe$_3$] or deamination of Ti(NMe$_2$)$_4$ to synthesise heterobimetallics [Cp*$_2$Zr(Me)(μ$_2$-O)Ti(Me)$_2$Cp*][153] and [Cp*$_2$Zr(Me)(μ$_2$-O)Ti(NMe$_2$)$_3$].[157] However, a mixture of species were observed from the reaction of [Cp*Zr(Me)OH] with 1 equivalent of Hf(NMe$_2$)$_4$; alongside [Cp*$_2$ZrMe(μ$_2$-O)Hf(NMe$_2$)$_3$], trimetallic [Cp*$_2$(Me)Zr(μ$_2$-O)Hf(NMe$_2$)$_2$(μ$_2$-O)Zr(Me)Cp*$_2$] was observed as a minor product. The trimetallic Zr_2Hf species is notable, as even the reaction of heterometallic [Cp*$_2$Zr(Me)(μ$_2$-O)Ti(NMe$_2$)$_3$] with a second equivalent of [Cp*$_2$Zr(Me)(OH)] still did not result in the formation of the trimetallic Zr_2Ti analogue. This reactivity difference may arise from the enhanced Brønsted basicity of Hf–NMe$_2$ units in comparison to Ti–NMe$_2$, due to the greater polarity of the Hf–N bonds, or from the steric bulk of the Cp* groups hindering a second deamination at the smaller Ti centre.[157]

The concept of dealkylation has also been applied to the incorporation of Mg–O–Zr units onto a Zr–containing MOF. Based on TPHN-MOF (TPHN = 4,4'-bis-(carboxyphenyl)-2-nitro-1,1'- biphenyl, Fig. 18), the deprotonation of terminal Zr$_3$(μ$_3$-OH) sites by $MgMe_2$ gave an elegant synthetic method to

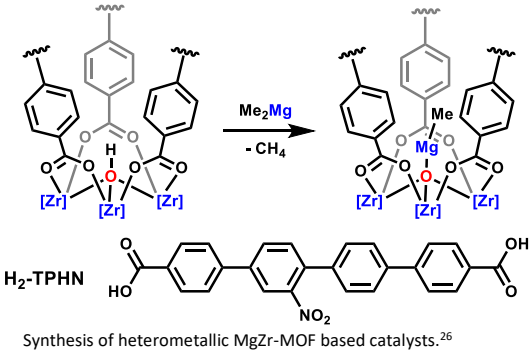

Fig. 18 Synthesis of heterometallic MgZr-MOF based catalysts.[26]

View Article Online
DOI: 10.1039/C8DT00017D

prepare MOF-based $Zr_3(\mu_4\text{-}O)Mg(Me)$ units. These materials were successfully applied as single-site catalysts for the hydroamination of carbonyls and imines, and for the hydroboration of aminopentenes. The steric bulk of the MOF ligand gives multiple advantages: the heterometallic catalyst can be reused (more than 10 times), and it prevents Schlenk-type ligand redistribution reactions, which are often observed with organomagnesium reagents.[26]

3.v Reactivity of Zn–OH complexes

The nature of the metal-hydroxide (M–OH) bond is important in facilitating its deprotonation by a Brønsted base (M'–R), as competitive side-reactions are also available. For example, metathesis of the hydroxide group can occur, to form stabilised M'–OH and M–R products. This has been reported for the reaction of precursor [$L_{MesNacNac}$Zn(OH)] with a range of organometallic reagents.[132] [$L_{MesNacNac}$Zn(OH)] was prepared through the controlled hydrolysis of [$L_{MesNacNac}$ZnMe] or [$L_{MesNacNac}$ZnH] with one equivalent of water. Subsequent deprotonation attempts were reported to be unsuccessful, even with strong Brønsted bases such as methyl-metal reagents LiMe, $AlMe_3$, Cp*$TiMe_3$, $ZnMe_2$, and aluminium reagents Al^iBu_3, Al^iBu_2H, and [$L_{dippNacNac}AlH_2$]. Instead, rapid metathesis reactions were observed, with exchange of the hydroxide and methyl/butyl/hydride groups (Fig. 19). While the formation of Zn–C or Zn–H bonds is surprising, this type of metathesis reaction is well-established in organic synthesis.[158] This study highlights the importance of selecting appropriate starting materials, as the difference in reactivity can be attributed to the weaker Brønsted acidity of the $L_{MesNacNac}$Zn–OH protons ([$L_{MesNacNac}$Zn(O*H*)], –0.2 ppm;[132] [$L_{dippNacNac}$Al(Me)(OH)], 0.53 ppm; Table 1).[140] Metathesis did not occur when aluminium and zinc were exchanged, so that the Brønsted acid was situated on aluminium. Instead, [$L_{dippNacNac}$Al(Me)(OH)] deprotonates [$L_{MesNacNac}$ZnH] upon prolonged heating, to form the heterometallic complex [$L_{dippNacNac}$Al(Me)(μ-O)Zn$L_{MesNacNac}$].

3.v Constructing Sn-O-M' connectivity from Sn–OH complexes

Mixed-metal Sn/Zn oxo clusters of general formula $[Sn(R_3)(\mu_3\text{-}O)ZnR']_4$ have been synthesised through the reaction of trimethyl or triphenyl tin hydroxide with dialkyl zinc reagents including $ZnMe_2$, $ZnEt_2$ and Zn^tBu_2 (Fig. 20).[24, 159] These tetramers possess $\{Zn_4O_4\}$ cubane cores, where the O are capped by terminal SnR_3 groups, structurally analogous to the alkyl-zinc-alkoxide heterocubanes, $[ZnR(OR')]_4$. These mixed-metal oxo clusters have been applied as single source precursors, to produce tin-doped ZnO NPs after thermal degradation under dry synthetic air. Notably, the tin concentration was tuneable, suggesting that heterometallic precursors provide a promising method of improving the properties of tin-doped ZnO materials.[24] Alternatively, metathesis routes can be applied to build Sn–O–M connectivity due to the greater stability of Sn–alkyl bonds in comparison to Al– or Ga–alkyl bonds.[160]

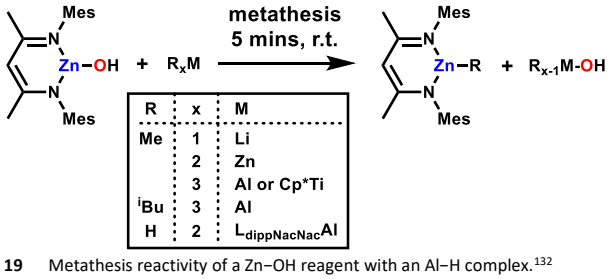

Fig. 19 Metathesis reactivity of a Zn–OH reagent with an Al–H complex.[132]

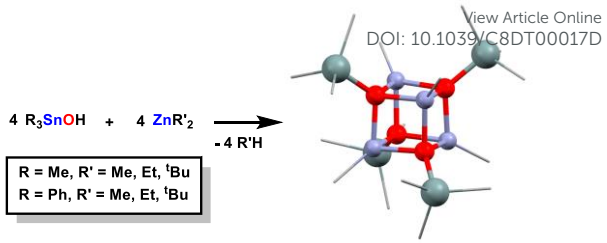

Fig. 20 Synthesis of $[Sn(R_3)(\mu_3\text{-}O)ZnR']_4$ heterocubanes.[24, 159] Colours: O, red; Zn, blue; Sn, grey.

A wide variety of complexes bearing M–O–M' units have been synthesised from M–OH precursors, utilising the highly basic nature of M–C or M–N bonds. However, the success of this route depends on the acid-base compatibility of the two reagents. The heterometallic systems which have been developed thus far highlight the trend of M–OH Brønsted acidity (Al–OH > Ga–OH > Zn–OH), with most systems developed from acidic Al–OH units. Most of the reported combinations are found when the organometallic reagent is strongly Brønsted basic (Mg, Al > Zn, Cu > Sn). This methodology is currently less established for less reactive metal pairings.

4. Hydrolysis routes to metal oxide nanoparticles

As metal oxides have diverse applications, many of which rely on surface properties, there has been great interest in building well-defined nanoscale versions with increased surface areas. Highly controlled synthetic protocols are required to design nanomaterials with narrow size distributions and/or to selectively favour a certain particle shape (e.g. spheres, disks or rods). Exposure of different facets of a metal oxide structure can affect the nanomaterial properties, which may be advantageous for the desired application, such as allowing a greater proportion of available active sites in catalysis or binding sites for sensors.[161, 162] Reduction of the nanocrystal size affects the electronic and optical properties. At particle sizes below the Bohr exciton radius, quantum confinement causes the band gap of a material to extend as the bulk solid begins to adopt a more localised or 'molecule like' electronic structure.[12]

Classical routes to metal oxide NPs involve the condensation of aqueous metal salts at elevated pH. Such routes require careful control of reaction parameters such as concentration and pH, along with choice of ligand and/or dopants, which often results in impurities within the product, and larger particle sizes – especially as Ostwald ripening processes occur readily in polar solvents.[163] Using an aqueous medium, the oxygen source (water) is always in excess, which removes the possibility of

View Article Online
DOI: 10.1039/C8DT00015D

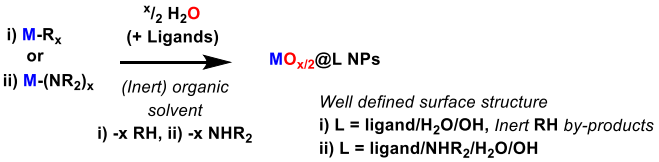

Fig. 21 Overview of dealkylation/deamination reaction of organometallic or metal-amide precursors with water to form metal oxide nanostructures.

stoichiometric control. To address these issues, extensive studies have been conducted upon non-aqueous sol-gel processes, to form metal-oxide nanostructures from soluble metal-alkoxide precursors in organic solvents.[97, 164, 165] Thermolysis and solvothermal routes can produce metal oxide NPs by 'non-hydrolytic routes', where the oxide anion comes from decomposition or reaction of the ligand and/or solvent, such as the release of ethers from metal alkoxides or esterification processes between carboxylic acid and alcohol ligands.[62, 165] As the oxygen source is again present in excess, the formation processes can be hard to study.

An attractive alternative route is to utilise highly reactive metal reagents (organometallics or metal-amides) which react readily with water in a direct stoichiometric reaction (Fig. 21). As the by-products may be inert (e.g. alkane from metal-alkyl precursors), this process can allow direct control of all factors of the NP synthesis: metal, oxygen, and ligand (both the type and concentration). This allows exceptional control and tunability of the NP surface chemistry. The hydrolysis pathway can be entirely controlled by the addition of water allowing for intermediary stages of hydrolysis to be studied in order to investigate the formation process.[96] The use of isotope labelled water ($H_2{}^{17}O$) enables straightforward and efficient synthesis of labelled metal-oxide NPs which may be studied by ^{17}O solid-state NMR techniques.[66] Further advantages include the low temperatures required for reaction (room temperature is typical), which place the synthetic process under kinetic control. Low temperature routes may be able to access metal oxide NPs with a large concentration of defects - it is well known that defects contribute extensively to material properties.[196, 197] Furthermore, formation of entirely new metastable metal oxide materials is a tantalising prospect. Polarz *et al.* described a low temperature (2°C) route to prepare a very unusual metastable phase of ZnO, which is described as akin to αBN. This unusual phase converts to the thermodynamic wurzite phase at 200 °C (Fig. 22a).[198] Kinetic control also favours the formation of small particles, as ripening processes can be retarded at lower temperatures. The use of organic solvents is also beneficial in this regard, as metal ions have low solubility restricting the rate of Ostwald ripening.

Hydrolysis of reactive metal precursors can take place under air, where both water vapour and O_2 can act as the oxygen source (*vide infra*). Several studies have indicated that water vapour is typically the key reagent under these conditions,[184, 189] however, the presence of oxygen may affect the products, especially where an oxidisable metal precursor is used (e.g. $Fe(N(SiMe_3)_2)_2$ or $Ni(\eta_4\text{-}C_8H_{12})_2$).[166] The scope of hydrolysis routes to NPs using organometallic or metal-amide precursors is shown in Table 2. While several metal oxide NPs have been prepared in this manner, there are opportunities to derive other oxides by such routes. By far the most studied material derived by M–C bond hydrolysis is wurzite ZnO, which proves to be an excellent example for studying the effects of ligand, solvent, and temperature upon the size, morphology, and surface structure of the resulting particles. Perhaps such interest in alkyl-zinc precursors for ZnO synthesis arises from their ready availability and good solubility in organic solvents (unlike $Zn(OR)_2$ species which form insoluble coordination networks). While this section will focus primarily on the hydrolysis of

Table 2 Synthesis routes to metal oxide NPs employing hydrolysis of reactive metal precursors. PVP = poly(vinylpyrrolidone).

Target Metal Oxide NP	Precursor	Ligands studied	NP sizes reported (nm)	Hydrolysis agent	Ref
γ-Fe_2O_3 (maghemite)	$Fe(N(SiMe_3)_2)_2$	Alkylamines, PVP	3-6	Air [or i) H_2O, ii) O_2] [11]	166, 167
$Fe_{(1-y)}O$ (wüstite)	$Fe(N(SiMe_3)_2)_2$	Hexadecylamine	5	H_2O	168, 169
Ni@NiO	$Ni(\eta_4\text{-}C_8H_{12})_2$	PVP	2.5-6	H_2O (and/or O_2)	170
Cu_2O (cuprite)	CuMes	Stearate, dioctylphosphinate	1-3	Air	171
CuO (tenorite)	[Cu(N,N'-diisopropylacetamidinato)]$_2$	Octylamine (reacts to form octylammonium octylcarbamate	4-15	Air	172
ZnO (wurzite)	$ZnEt_2$	Carboxylates, dioctylphosphinate, polyetherpolyols, carboxylate-PEG chiral-aminoalcohol	2-7	H_2O, Air	96, 173-183
	$ZnCy_2$	Alkylamines, carboxylates, amino-PEG, hyperbranched polymers	2-10 + Rods <120 nm long[184]	Air	184-188
	$Zn(N^iBu_3)_2$	Hexylamine (reacts to form hexylammonium hexylcarbamate)	3-5	Air	189
	$Zn(N(SiMe_3)_2)_2$	No added ligand	15	H_2O	190
	[ZnR(OR')]$_4$ R = Et, R' = C_4H_7O; R = Me R' = Me, Et, ^iPr, ^nPr, ^iBu, ^tBu	No added ligand, polyglyceryl-3-polyricinoleate	7-22 Rods (95 x 10^{191}, 50 x17^{192})	H_2O	191-193
ZnO (αBN phase)	[ZnMe(O^tBu)]$_4$	PVP, palmitic acid	N/A	H_2O (2°C)	23
$Sn_3O_2(OH)_2$ (oxidises to SnO_2 at 500°C)	$Sn(NMe_2)_2$	Hexadecylamine	3-5	H_2O	194, 195

View Article Online
DOI: 10.1039/C8DT00017D

reactive precursors (Fig. 21), it is worth noting an alternative stoichiometric strategy to metal oxide NPs by low temperature routes - the 'direct liquid phase participation' pathway developed by Morris and co-workers.[199] In this case, the oxygen source is Na_2O, which reacts with a MCl_x precursor in a direct stoichiometric manner in alcohol solvents. Whilst the metal oxide phase precipitates as small NPs the by-product NaCl remains dissolved in the alcoholic solution. The process can be used for a variety of metal oxide products such as Cu_2O, WO_3 or even ternary phases such as $CoFe_2O_3$,[199, 200] with additives (e.g. alkylamines and oleic acid) enabling improved monodispersity of the NPs.

The production of nanoparticulate metal oxides allows for these materials to be transferred to the solution phase, particularly useful for liquid processing techniques or for conducting chemistry in a pseudo-homogeneous phase.[171] For example, traditional heterogeneous catalysts may be transferred to a colloidal phase, enabling different approaches to reactor design, with potential advantages such as better control of temperature gradients and reduction of detrimental 'hot-spots' within the reactor.[201] Surface ligands (or surfactants) are required to stabilise and solubilise NPs; these ligands can be selected to direct the particles into a chosen solvent medium (e.g. amphiphiles allow solvation in organic solvents, whilst polyethylene glycol (PEG) chains can give good solubility in water).[186, 187] The choice of ligands also affects the synthetic process and resulting particle morphology. Both neutral Lewis basic (e.g. amine) and anionic (e.g. carboxylate) ligands may be coordinated to a metal oxide surface. Strongly binding ligands (which are typically anionic) can be used in substoichiometric quantities relative to the metal, allowing for a greater degree of the metal oxide surface to be exposed.[174, 202] Alternatively, less strongly bound neutral ligands may show a reversible binding nature allowing indirect access to the metal oxide surface.[203, 204] The hydrolytic routes discussed here typically result in hydroxide/water terminated surfaces, as evidenced by spectroscopic techniques.[205]

Metal oxide NPs produced by hydrolysis of reactive precursors have found a range of applications including the pseudo-homogeneous catalytic reduction of CO_2 to MeOH (ZnO and Cu NPs);[173, 202, 206, 207] polymeric antibacterial surfaces (ZnO);[208, 209] photocatalysts (ZnO);[183, 210] gas sensors (ZnO,[211] SnO[194, 195], CuO[172]); photoconductive UV detectors (ZnO);[212] and MRI contrast agents (γ-Fe_2O_3).[167] The ability to control size, morphology, surface chemistry and ligand coverage has proved very valuable in producing NPs for these applications.

These hydrolysis reactions are not restricted to organic solvent media - in fact, a range of different reaction conditions have been employed to produce NPs embedded within gels, composites, and mesoporous materials. Polarz and co-workers prepared a ZnO-containing aerogel which exhibited photocatalytic properties by slowly hydrolysing a range of $[ZnMe(OR)]_4$ heterocubanes in diglyme at 0°C and subsequently (supercritically) drying the gel.[210] The same research group extended their work on heterocubanes to utilise the precursor $[ZnMe(OCH_2CH_2OCH_3)]_4$ which is liquid at room temperature but has a high boiling point, and is therefore easily added into mesoporous supports. The liquid heterocubane was hydrolysed in moist air inside a mesoporous silica host to produce crystalline ZnO NPs (~5nm). These NPs were slightly smaller than those prepared outside the confines of the host, supporting the growth of NPs within the mesopores.[213] The same Zn precursor was also shown to be effective in building ZnO networks around carbonaceous supports by hydrolysis in humid air; once the support was removed (by oxidation at >500°C) a mesoporous ZnO structure was obtained. Janssen and co-workers hydrolysed spin coated mixtures of $ZnEt_2$ and a conjugated polymer, poly[2-methoxy-5-(3',7'-dimethyloctyloxy)-1,4-phenylene vinylene], in air at room temperature to produce photoactive films which could be fashioned into hybrid bulk-heterojunction solar cells, although an annealing step (110°C) was required to generate crystalline ZnO for enhanced performance.[214] Williams, Shaffer, and co-workers described the formation of thermoset composite materials comprising ZnO NPs (5-40 weight %) embedded in epoxy resin.[215] The $ZnEt_2$ precursor does not react with the epoxy prepolymer (Araldite) while under inert atmosphere and undergoes a hydrolysis reaction with wet acetone to generate ZnO NPs and ethane. The ZnO/prepolymer mixture was then cured at 120°C with a diamine hardener to produce a resin. Remarkably, both the hydrolysis procedure and resin chemistry occur without affecting each other; in contrast, a more traditional base-assisted NP synthesis route was shown to destroy the prepolymer.[174, 215] The same $ZnEt_2$ hydrolysis method can be used to form ZnO NPs upon carbon nanotube surfaces, a process that may also be conducted in a prepolymer medium in order to produce further hierarchical composite materials.[215] Kahn and co-workers described the hydrolysis of $ZnCy_2$ dissolved in a liquid crystal medium. The resultant ZnO NPs are influenced by the state of the liquid crystals, with the (lower temperature) nematic phase of the liquid crystals supporting growth of ZnO nanoworms or nanowires up to 200 nm in length. In contrast, small (<6 nm) isotropic ZnO NPs are formed at higher temperatures, as local order is disturbed throughout the liquid crystal.[216]

Considering reactions in air, it is useful to determine the oxygen source, which could be H_2O or O_2. While hydrolysis of ML_x (L = R or NR_2) cleanly generates M−OH_x and L−H (x equiv.), allowing subsequent condensation to metal oxides, the reaction with oxygen can lead to more complex reaction processes. Insertion of dioxygen can occur into M−C bonds to form peroxo species (M−OOR), and these unstable complexes may rearrange to form alkoxides.[47] For example, the reaction of $ZnMe_2$ with O_2 was shown to form the biscubane structure $Zn_7Me_6(OMe)$.[217] Alternatively, reductive coupling may occur, as shown in the reaction of a controlled amount of O_2 with CuMes to form $Cu_{10}Mes_6O_2$ and Mes−Mes.[218] This process productively builds M−O−M bonds but is generally a less favourable reaction compared to hydrolysis with water vapour. Various studies have addressed the difference between O_2 and H_2O as oxygen sources - the reaction of (amine coordinated) $Zn(Cy)_2$ with moisture produced nanorods, the same result as when the reaction was conducted under air.[184] However, under dry O_2 the reaction gave less well-defined NPs of ZnO, indicating that

moisture was the more influential component of air. These studies noted no evidence for Zn−OH intermediates, suggesting that the exothermic hydrolysis process rapidly drives condensation to ZnO.[184] Gladfelter and co-workers also showed that moisture was the major reagent in the reaction of $Zn(N^iBu_2)_2$ under air.[189] The ZnO NP size increased as the humidity level was increased, while only amorphous products were formed under dry conditions. The presence or absence of O_2 may still be important in the hydrolysis reaction: for example, the reaction of $Fe(N(SiMe_3)_2)_2$ with water forms wüstite $Fe_{1-y}O$ NPs;[168, 169] whilst under air the iron becomes oxidised, instead forming maghemite Fe_2O_3 NPs.[166] Furthermore, employing a stepwise process, where oxidation is undertaken subsequently to hydrolysis, results in higher-quality superparamagnetic Fe_2O_3 NPs, indicating the importance of controlling both hydrolysis and oxidation pathways.[167] If the absence of oxygen is required, water must be added to the precursor solution. A water miscible solvent such as acetone or THF may be used as a medium to disperse the required water and is useful for mixing moisture into non-polar solvents such as hexane or toluene.[173, 174, 193] Alternatively reaction at a cyclohexane/water interphase has also been reported for the hydrolysis of $[ZnMe(O^iPr)]_4$.[192]

A particular advantage of stoichiometric hydrolysis is the ability to study the reaction process in detail by the stepwise addition of reagents. As reactions occur at room temperature, such processes are straightforward to study in real time. The mechanism of NP nucleation and growth has interested researchers for many years, as understanding such processes is key to designing synthetic protocols to target monodisperse NPs of the desired morphology and surface structure. In this section, three examples of ZnO NP formation will be reviewed focusing on the mechanism of hydrolysis in each case: i) no added ligand, ii) weakly binding ligands in excess, and iii) strongly binding ligands (which may be used in substoichiometric quantities).

4.i.a Hydrolysis of heterocubanes $[ZnR(OR')]_4$

The hydrolysis of heterocubanes $[ZnR(OR')]_4$ has been studied extensively by the groups of Driess and Polarz. This synthetic route is often undertaken without an additional ligand, although it should be noted that since these precursors contain both M−R and M−OR functionalities, residual (H)OR groups may stabilise the NP surface. NMR and Raman spectroscopies revealed that, despite expectations, water preferentially reacts with the Zn−OR' bond instead of the Zn−C bond, which may be kinetically favoured due to initial proton transfer to the available OR lone pair.[52] This reactivity supports the formation of an intermediary precursor containing Zn−OH functionality, which may maintain the original cubane geometry.[193] In support of this, a range of $[Zn^tBu(O^tBu)_{(1-y)}(OH)_y]_4$ (y = 0-3) have recently been structurally characterised by Lewiński and co-workers.[219] The Zn−OH units can then dealkylate Zn−R to form Zn−O−Zn networks. The rate of NP formation is dependent upon the Zn−OR functionality, with bulky groups slowing hydrolysis. Studies of the nucleation process in THF indicate that critical nuclei of 1.5-2 nm wurzite ZnO form directly via supersaturation of the solution with the molecular precursors. A slower growth process follows, allowing formation of larger (~8 nm) NPs. The solvent plays an important role in the eventual particle size, with non-polar solvents favouring larger particles – this supports a supersaturation mechanism, where the solubility/stability of the forming ZnO critical nuclei (which have polar facets) compared to the (hydroxy)-precursor is key.

Whether the original cubane geometry influences the growth of wurzite ZnO NPs is an intriguing question.[220] The cubane structure does not closely correlate with the hexagonal wurzite structure, suggesting significant internal rearrangement must occur to convert to the extended ZnO phase. Driess and co-workers have synthesized $Zn_xR_y(OR)_z$ precursors of different nuclearity (x = 1, 2, 4 or 7) and found that the mononuclear Zn precursor $ZnEt(O(2,6\text{-}C_6{}^iPr_2H_3))py_2$, which was stabilised by coordinated pyridine solvent, hydrolysed to irregular ZnO spheres (>10 nm).[191] However, all the higher nuclearity precursors (x = 2, 4 or 7) progressed to form ZnO nanorods, hinting that the precursor can influence the NP morphology. It is important to note that in this example the various precursors contained different OR groups with a range of steric demands, which may also play a role in dictating the NP morphology. Polarz and co-workers produced a new metastable αBN-like phase of ZnO stabilised by PVP from $[ZnMe(O^tBu)]_4$ (Fig. 22a).[198] In this phase, hexagonal sheets of ZnO are alternately stacked directly above each other so each atom is 5 coordinate. Again, the question of whether the cubane precursor may condense directly into this structure remains. Some degree of bond breaking is still required to generate the αBN structure, and instead the cubane might be expected to generate a rock salt

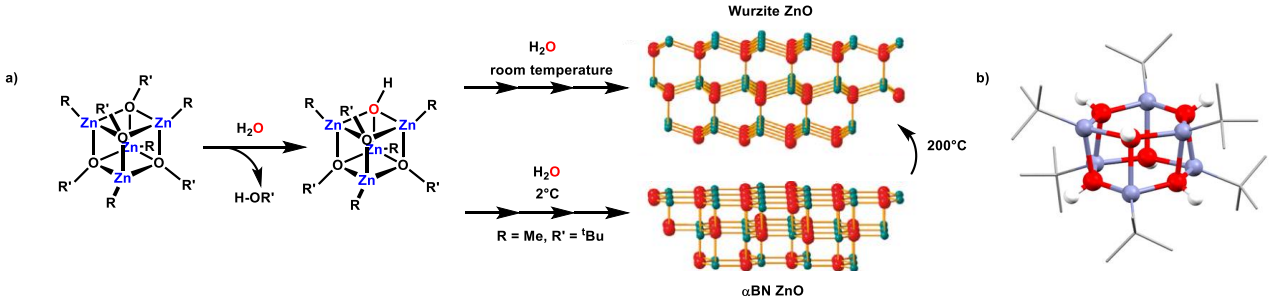

Fig. 22 a) structure of $[ZnR(OR)]_4$ heterocubanes and their hydrolysis pathway to ZnO nanomaterials, figure adapted with permission from the American Chemical Society[198] b) the solid-state structure of a hexagonal prismatic $[Zn^tBu(OH)]_6$ cluster displaying the possibility of pre-arranging hexagonal clusters before condensation.[83]

View Article Online
DOI: 10.1039/C8DT00017D

ZnO structure. Interestingly, Lewiński and co-workers prepared a metastable hydroxide cluster $[Zn^tBu(OH)]_6$ which is shaped as a hexagonal prism (Fig. 22b).[83] Since it has been suggested that $[ZnR(OR')_y(OH)_{1-y}]_x$ clusters[219] form from the initial hydrolysis of the cubanes, it seems plausible that subsequent equilibration to a hexagonal structure may occur, which could then condense into the αBN phase. A 2D αBN ZnO phase was also identified as an intermediate to wurzite ZnO nanosheets when the hydrolysis of $[ZnMe(OBn)]_4$ was conducted in ionic liquids.[221]

4.i.b Effects of amine ligands upon ZnO NP formation

The presence of external ligands is likely to change the precursor complexes and the route of hydrolysis. Chaudret, Kahn, Maisonnat, and co-workers have extensively studied the hydrolysis of $Zn(Cy)_2$ in the presence of long chain alkyl amines under air, resulting in wurzite ZnO NPs and nano-rods, which exhibit good solubility in organic solvents (Fig. 23).[222] The initial formation of $Zn(Cy)_2(NRH_2)$ Lewis adducts is clearly shown by NMR spectroscopy.[185, 188, 203] At least one equivalent of amine is required to produce homogeneous nanomaterials, and larger excesses of amine ligand promote the growth of longer nano-rods. Without using additional solvent, a high concentration of amine promotes nano-rod formation, but only when hydrolysis is conducted below 60°C.[188] Above this temperature isotropic ZnO NPs are produced, indicating the critical importance of ligand organisation during the formation process. Longer chain alkylamines also favour rods, whilst shorter chains may produce spherical particles.[184] When utilising amino-PEG ligands, varying the ligand:metal ratio affected the size and monodispersity of the resultant ZnO (0.05 equiv. ligand, ZnO = ~7 nm; 2 equiv. ligand, ZnO = ~4 nm).[186] These factors indicate that the ligand plays an important role during the synthesis process.[184] NMR studies reveal that in the resulting ZnO NPs, the amine ligands are loosely bound in solution and undergo dynamic processes exchanging between three states: surface coordinated, loosely interacting, and non-coordinated (Fig. 23b).[203] Due to the versatility of the synthetic protocol, water soluble ZnO NPs were also prepared with amino-PEG ligands; zeta potential techniques studied the surface charges of these ZnO NPs and showed that they are primarily stabilised by ligand sterics and not by a significant colloidal charge.[186] Gladfelter and co-workers showed that during the hydrolysis of $Zn(N^iBu_2)_2$ and hexylamine under air, the ligands react with atmospheric CO_2 to form hexylammonium hexylcarbamate. The authors show an approximate 1:1 ratio of hexylammonium and hexylcarbamate but suggest slight excess of either species could help to quench any surface charges upon the ZnO surface.[189] Kahn, Maisonnat, and co-workers present a similar scenario by mixing oleic acid (0.5 equiv. to Zn) with alkylamines (1 equiv. to Zn) to produce a ligand system containing alkylammonium carboxylate ion paired ligands; this system was adept for forming self-organised superlattices of monodisperse ZnO NPs.[223]

4.i.c Synthesis of ZnO NPs with strongly bound anionic ligands

Anionic ligands (e.g. carboxylates or dialkylphosphinates) bind to surface Zn cations upon a ZnO NP. The reaction between an

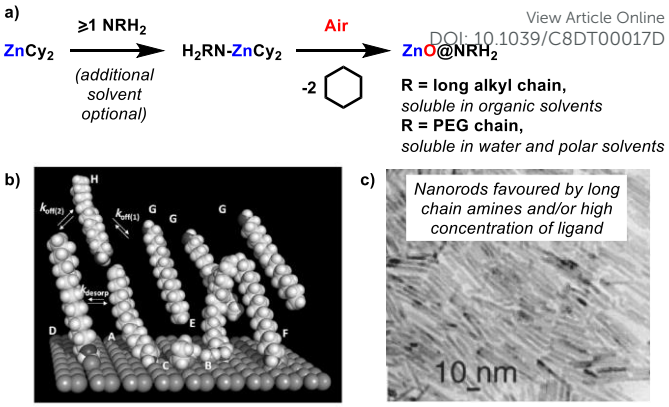

Fig. 23 a) Hydrolysis of $ZnCy_2$ with amine ligands under air. b) Reprinted with permission from John Wiley and Sons;[203] illustration of the various interactions at the surfaces of the ZnO NPs. Amine (A), H_2O (B), and THF (C) molecules coordinate to Zn^{2+} ions; amine groups hydrogen bond to a hydroxy group (D) and to a H_2O molecule at the surface (E); amine groups coordinate to Zn^{2+} ions and hydrogen bond to a H_2O molecule at surface (F); second-shell ligands (G); free amine in solution (H). c) reprinted with permission from John Wiley and Sons;[184] ZnO@octylamine nanorods formed from hydrolysis of $ZnCy_2$ and 2 octylamine without additional solvent.

acidic pro-ligand (e.g. carboxylic acid) and a Zn–alkyl results in a polar covalent Zn–ligand bond, which is not readily hydrolysed by water. The groups of Williams, Shaffer, and Lewiński have studied such ZnO@ligand NPs produced by the hydrolysis of $ZnEt_2$.[96, 173, 174, 176-179, 208, 209] Lewiński and co-workers employed a simple 'one-pot, two-step' strategy of exposing a THF solution of ligated precursor $[ZnEtL]_n$ (L = $[RCO_2]^-$, $[R_2PO_2]^-$ or aminoalcoholate) to air, producing small (~2-8 nm) ZnO@L NPs with a dense surface coverage of ligand.[176, 178, 179] This synthetic route yields ZnO NPs described as $(ZnO)_x(ZnL_2)_y(L)_z$ (L = monoanionic ligand) with more than a single monolayer of ligands. This ligand shell is described as 'impermeable', and protects the ZnO core, which results in slow photoluminescence (electron-hole separation up to 2.2 μs)[180], giving these NPs enhanced properties relative to ZnO from sol-gel techniques.[179] The process tolerates many different R groups upon the anionic ligand (Fig 24), for instance, the use of liquid crystalline carboxylates such as $O_2CC_6H_4OC_{12}H_{25}$ allowed the preparation of ZnO NPs which self-assemble into free-standing thin films when compressed upon an air-water interface by the Langmuir method.[176, 182] The films form via ligand interdigitation and retain the photoactivity of the individual ZnO NPs. Further studies showed that a Cu catalysed alkyne-azide cycloaddition reaction may be subsequently initiated on ZnO with alkyne terminated carboxylate ligands, and, unlike other NP preparation routes, these NPs remain luminescent after exposure to the Cu(I) catalyst, due to the as the impermeable surface layer of ligands.[177] Similarly, water soluble ZnO NPs (stable in the pH range 3-9) showed low mammalian toxicity attributed to the surface protection of the ZnO core which prevents leaching of Zn^{2+}.[179]

In other scenarios access to the ZnO surface is required, and so a lesser amount of ligand is desirable. This can be easily adjusted when using an organometallic precursor as no coordinating by-products are produced. For example, reducing

View Article Online
DOI: 10.1039/C8DT00045D

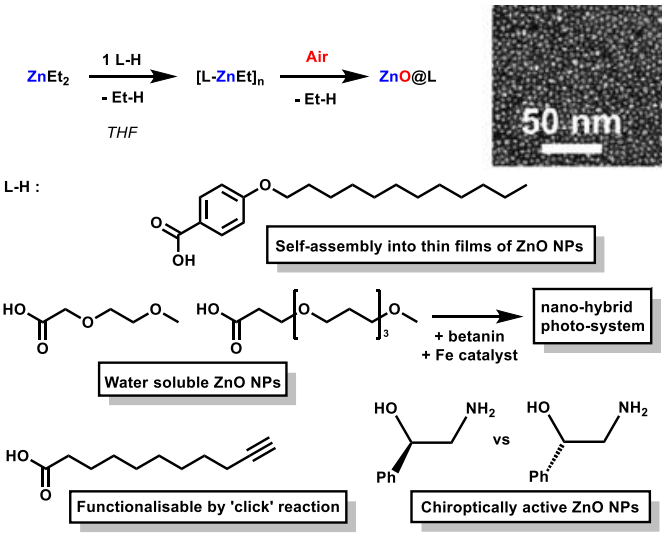

Fig. 24. Versatile 'one-pot, two-step' synthesis route to carboxylate or amino-alkoxide functionalised ZnO NPs (~2-8 nm, dependent on ligand choice) with a dense ligand shell (1:1 ligand:Zn). Different ligand precursors lead to NPs with a variety of properties and applications.[176-183] TEM micrograph reproduced with permission from the RSC.[177]

the amount of ligand is helpful in forming composite materials, where excess ligand would affect the material properties, e.g. causing plasticization. The ability to control ligand concentration is also valuable as the surface chemistry of NPs may be determined by the surrounding ligands, which may impose steric or electronic effects upon the NP surface.[224-226] Reducing the ligand surface coverage may allow a greater proportion of the NP surface to be available to reactants – key in applications such as catalysis or sensing.[226-228] For example, a recent study employing the combination of ZnO and Cu NPs to make hybrid nano-catalysts for the hydrogenation of CO_2 to methanol, reported that lesser amounts of ligand allowed ZnO/Cu interfaces to form, which are believed to be important for generating catalytically active sites.[202]

Williams, Shaffer, and co-workers reported that mixing various ratios of $ZnEt_2$ and Zn(stearate)$_2$ in toluene leads to the formation of a pentanuclear species, $Zn_5Et_4(OOCR)_6$, alongside excess $ZnEt_2$.[229, 230] These mixtures were subsequently hydrolysed with either water or humid air.[174] A rapid hydrolysis pathway occurred using water, which produced 3-4 nm ZnO@stearate NPs with a low size dispersity, spherical shape, and good solubility in organic solvents. Variation of the ligand stoichiometry from 0.05-0.33 equiv. (relative to total Zn) did not significantly affect the NP size (Fig. 25), suggesting that the particle size is mainly determined by the nucleation step. Ligand loadings of <0.2 equiv. (relative to Zn) produced ZnO NPs with ligand surface coverage estimated to be less than 100%. Further reducing the ligand loadings to 0.05 equiv. gave partially covered NPs (<15% surface coverage) which exhibit lower solubility in toluene. Higher ligand loadings (e.g. 0.33 equiv.) resulted in the formation of Zn(stearate)$_2$ alongside the ZnO NPs. Intriguingly, when humid air is employed as the moisture source instead, and the hydrolysis occurred more slowly, the ligand stoichiometry does affect the particle size: larger (<7 nm) ZnO NPs formed using lower proportions of ligand (0.05 equiv. to Zn) (Fig. 25), although a greater size dispersity was noted. The stearate ligands were shown to adopt a variety of surface coordination modes, although a bridging mode was most common.[205] As incomplete surface coverage is possible in this system, remaining surface sites may be OH terminated, consistent with broad signals in the IR spectra at 3400 cm^{-1}.[174, 205] Even in ZnO@stearate NPs with almost complete surface coverage (0.2 equiv. ligand relative to Zn), adsorption of CO_2 was observed at ambient temperatures, showing that the ligand shell does not block access to the NP surface.[205]

Dioctylphosphinate ([DOPA]$^-$) exhibits a similar bridging anionic coordination mode to carboxylates. The precursor, dioctylphosphinic acid can be used directly with $ZnEt_2$ in a substoichiometric ratio to produce a precursor solution containing $[ZnEt(DOPA)]_4$ along with excess $ZnEt_2$.[96, 173]

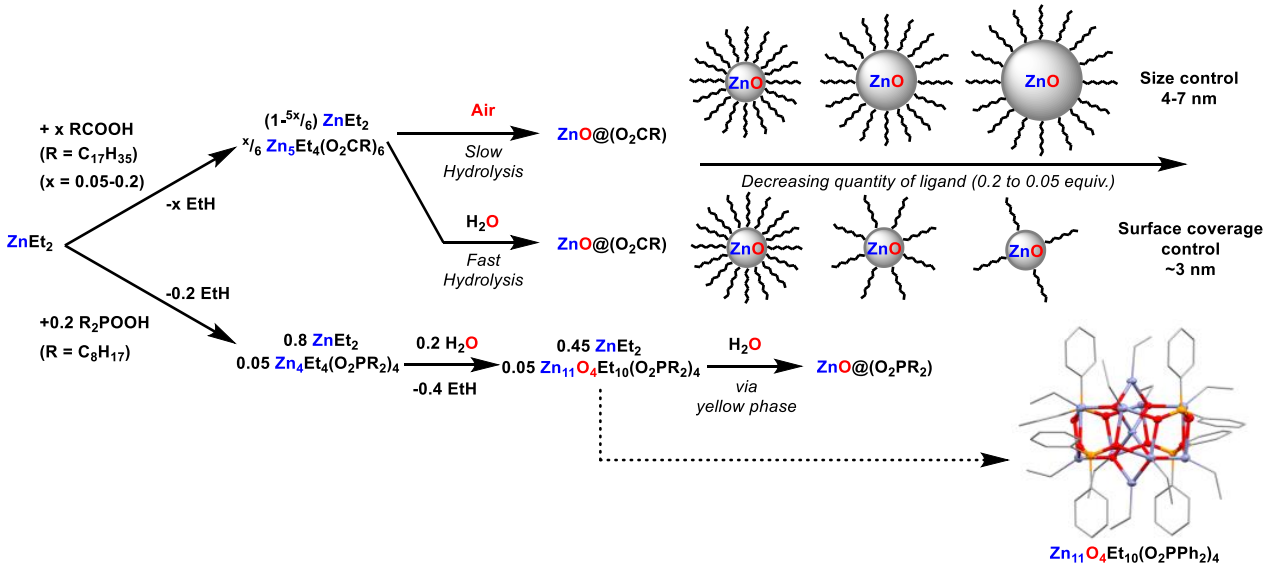

Fig. 25 Reaction of $ZnEt_2$ with ≤0.2 equiv. of carboxylic acid or phosphinic acid proligands and subsequent hydrolysis to ZnO NPs.[96, 174, 229] The solid-state structure of $Zn_{11}O_4Et_{10}(O_2PPh_2)_4$ is displayed, which is a structural model for the spectator cluster $Zn_{11}O_4Et_{10}(O_2P(C_8H_{17})_2)_4$ observed during hydrolysis with dioctylphosphinate ligands. Colours: O, red; Zn, blue; P, orange.

View Article Online
DOI: 10.1039/C8DT00017D

Hydrolysis of the mixture with water generates ZnO@DOPA particles with similar sizes and properties to the ZnO@stearate particles; however, the incorporation of a ^{31}P nuclei allowed the hydrolysis process to be studied in detail by multinuclear NMR spectroscopic techniques. Monitoring the reaction of $ZnEt_2$ and dioctylphosphinic acid (0.2 equiv.) in d_8-toluene by ^{31}P NMR showed the formation of $[ZnEt(DOPA)]_4$ along with excess $ZnEt_2$, which rapidly reacted with water to produce a partially hydrolysed Zn cluster, $[Zn_{11}Et_{10}O_4(DOPA)_4]$, as the major product after 37.5% hydrolysis of Zn−Et bonds (Fig. 25). Such Zn_{11} clusters have been shown to exhibit equilibrium relationships with $ZnEt_2$ and other Zn clusters, suggesting a dynamic equilibrium-based rearrangement occurs under partial hydrolysis conditions. Remarkably, this Zn_{11} cluster sequesters all available $[DOPA]^-$ ligand and is retained as hydrolysis continues, essentially acting as a spectator to the nucleation of the remaining $ZnEt_2$. After formation of the Zn_{11} cluster, further hydrolysis (from 37.5-75%) causes a colour change to yellow, although little change is observed in the ^1H or ^{31}P NMR spectra (except from the loss of $ZnEt_2$ resonances). *In-situ* UV/vis studies suggested that no well-defined ZnO NPs are present during this stage of hydrolysis, as no characteristic band edge absorption is located. The yellow phase is thus described as highly defective/ disordered amorphous unligated ZnO NPs. This yellow phase has also been noted during the partial hydrolysis of $ZnEt_2$ in the absence of added ligands, and in the hydrolysis of other $Zn(alkyl)_2$ species.[223] Only on reaching completion of the hydrolysis process is the Zn_{11} cluster consumed, the yellow colour lost, and the typical absorption spectrum for ZnO NPs revealed (NP size = 2-3 nm), indicating a re-equilibration of the mixture to form ZnO@DOPA NPs. Whilst the $[DOPA]^-$ ligand is essential for producing well defined NPs with good solubility, ZnO NPs of a similar size (3.5 nm) may be produced without ligand by the same hydrolysis process. Such results are consistent with the concept of a nucleation-driven NP synthesis, in which the anionic ligand does not obviously affect the nucleation or the resulting particle size. This contrasts with the size and shape control found when using neutral amine ligands. In the ZnO@DOPA synthesis, the connectivity of ligated molecular precursors appears to have little effect on the reaction trajectory or products. For these strongly bound anionic ligands, NMR spectroscopic techniques do not reveal ligand exchange processes upon the ZnO NPs, suggesting a well-defined, static surface coordination in comparison to the more loosely bound neutral amine ligands.[96, 203, 231]

4.ii Doped or Mixed-Metal Oxide Nanoparticles

Tailoring properties by doping is a key strategy in material design, however, doping nanomaterials can be challenging due to the possibility of phase separation. Differential rates of hydrolysis are likely to lead to condensation of separate metal-oxide phases, and in aqueous synthetic routes the precursor may condense at different pH values. The use of heterobimetallic precursors is a useful technique for intimately incorporating multiple metals into a bulk structure.[111, 233] Metal alkoxides have been successfully utilised as precursors for mixed-metal oxide films and powders, they dissolve well in organic solvents and precursor sols may benefit from ether elimination reactions to form mixed-metal oxo bridged precursors.[234] However, differential rates of hydrolysis can be problematic - in some cases this can be circumvented by using non-hydrolytic routes.[62] If using organometallic or metal-amide precursors, intimate doping is also reliant on similar rates of hydrolysis for all precursors, yet good solubility and low reaction temperatures may be beneficial in these systems. Atomic layer deposition techniques targeting doped metal oxides have been reported using organometallic/metal-amide precursors which are hydrolysed *in situ*.[235] The synthesis of well-defined doped or mixed-metal oxide NPs from organometallic/metal-amide precursors is yet to be explored in detail, however, routes to Li and Mg doped ZnO NPs have been reported (table 3).

Chaudret, Kahn, and co-workers utilised group 1 metal-amides as growth-controlling agents in the hydrolysis of $ZnCy_2$ with octylamine.[67] Without dopant, this route produced ZnO nanorods. However, the addition of Li-amides led to small spherical (wurzite) NPs which became smaller with increasing Li content (1-10% doping was tested, with a size decrease of up to 30% observed). As the covalent radii of Li is similar in size to Zn (Li, 1.23 Å; Zn, 1.25 Å), the authors propose that LiOH condenses onto the surface of growing ZnO NPs, hindering further growth and forming a Li rich surface layer.[67] This results in a blue shift of the luminescence of the doped NPs. More recently, Polarz and co-workers prepared highly crystalline Li doped ZnO nanorods by using an oil in water emulsion technique, in which the Zn precursor is added to the oil phase with Li salts dissolved in the aqueous phase.[232] Amorphous gel-like particles are initially formed, which crystallise into clusters of wurzite nanorods; the authors propose that this unusual growth process benefits from intimate doping as the Li ions are trapped in the vicinity of the growing ZnO structure. A single ^7Li solid-state NMR resonance was identified suggesting that Li^+ is replacing Zn^{2+} within the lattice. A new EPR signal was also observed, characteristic of heteroatoms occupying Zn^{2+} sites. Mg doped ZnO NPs may be formed by mixing $ZnEt_2$ with $MgBu_2$ before hydrolysis in the presence of dioctylphosphinic acid. The resultant particles showed only the wurzite phase by powder X-ray diffraction at a 10% Mg doping level, suggesting that Mg is fully incorporated into a typical ZnO structure.[209]

Table 3. Synthesis routes to doped metal oxide NPs utilising reactive metal precursors

Target Metal Oxide NP	Doping Content (%)	Precursors	Ligands studied	NP sizes reported (nm)	Hydrolysis agent	References
Li doped ZnO (wurzite)	1-10%	$ZnCy_2$ + $Li(N(SiMe_3)_2)_2$ or $Li(NMe_2)$	Octylamine	2.5-4.3	Air	67
Li doped ZnO (wurzite)	10%	$[MeZn(OiPr)]_4$ + $Li(O_2CR)$	Stearate	Rods 15x200	H_2O	232
Mg doped ZnO (wurzite)	10%	$ZnEt_2$ + $Mg(^nBu)(^sBu)$	Dioctylphosphinate	3	H_2O	209

View Article Online
DOI: 10.1039/C8DT00017D

5. Summary and Outlook

The reaction of highly Brønsted basic organometallic or metal-amide complexes with protic OH groups provides a promising strategy to form a variety of metal-oxo structures ranging from molecular M−O−M' species to nanomaterials. These synthetic routes have enabled the formation of oxo-bridged heterometallic species that act as highly tuned catalysts for polymerisation reactions,[25] and of metal oxide NPs which have found uses in a variety of applications including catalysis,[202] sensing,[195] and antibacterial surfaces.[208] Controlled reactivity with water also allows the formation of partially hydrolysed metal-oxo cluster species. These clusters are of interest as the molecular relations of metal oxide materials - studies on such clusters have shed light on the stability of MOFs[104] and the mechanisms of metal oxide NP formation.[96]

As organometallic/metal-amide precursors react rapidly at room temperature, hydrolysis reactions can be straightforward, occurring even just from exposure to air. Such low temperature reactivity enables access to kinetic products and previously unknown metastable oxide phases.[198] Unlike alternative sol-gel routes, the hydrolysis of organometallics yields alkane or arene by-products which are chemically inert (and may be gases), allowing for clean reactivity and excellent control of surface chemistry in NPs.[174] In contrast, metal-amides hydrolyse to generate amines, which can act as stabilisers in NP synthesis.[190] Organometallic reagents typically have good solubility in organic solvents, making them excellent reagents for solution phase chemistry - in contrast to poorly soluble M(II) alkoxides. Whilst organometallic reagents are often highly reactive to air and moisture, in some cases they display higher stability than the related alkoxides. For example, CuMes is a versatile reagent in contrast to thermally unstable Cu(I) alkoxides. A broad range of organometallics and metal-amides are commercially available or may be straightforwardly synthesised.

Ligands also influence the hydrolysis of metal precursors. Neutral or anionic ligands can alter the electronics, sterics and aggregation state of organometallic/metal-amide reagents to influence their basicity. Ligands can also affect the acidity and stability of metal-hydroxide complexes, such as those which dealkylate organometallics to form homo- or heterobimetallic structures.[132] While ligands may appear strongly bound, evidence shows that exchange and equilibration can readily occur during hydrolysis, and any structural identity of clusters is often reordered during reaction. For covalently bound ligands, small metal:ligand ratios typically produce small ligated metal-oxo clusters, while greater proportions of metal may generate larger structures. Divergent reactivity to produce ligated metal-oxo clusters alongside metal oxide may also occur if the ligated species is less moisture sensitive than its parent organometallic precursor, as is key in the formation of ZnO@(phosphinate) NPs.[96] Neutral ligands also play an important role in NP synthesis and may direct the growth of nanorods.[188]

The focused use of certain metals for different research areas is highlighted throughout this discussion, for example organo-aluminium/gallium reagents have been used to form a variety of molecular metal-oxo clusters;[73, 75] group 4 metals are commonly found in oxo-bridged dimers;[153] and organozinc species form versatile reagents for ZnO NPs.[96] There is scope for future discoveries to blur these boundaries, and to test different organometallic or metal-amide precursors for the formation of new molecular oxo species, clusters and NPs.

Conflicts of interest

There are no conflicts to declare

Acknowledgements

JAG acknowledges the Christina Miller Fellowship Fund. SDP acknowledges the Herchel Smith Postdoctoral Fellowship Fund.

References

1. S. B. Ogale, T. V. Venkatesan and M. G. Blamire, *Functional Metal Oxides: New Science and Novel Applications*, Wiley-VCH, Weinheim, Germany, 2013.
2. J. L. G. Fierro, *Metal Oxides: Chemistry and Applications*, CRC Press/Taylor & Francis Group, Boca Raton, Florida, 2006.
3. B. O'Regan and M. Gratzel, *Nature*, 1991, **353**, 737-740.
4. A. Fujishima, T. N. Rao and D. A. Tryk, *J. Photochem. Photobiol., C:*, 2000, **1**, 1-21.
5. W. Zhong Lin, *J. Phys.: Condens. Matter*, 2004, **16**, R829.
6. S. C. Dixon, D. O. Scanlon, C. J. Carmalt and I. P. Parkin, *J. Mater. Chem. C*, 2016, **4**, 6946-6961.
7. A. Asati, S. Santra, C. Kaittanis, S. Nath and J. M. Perez, *Angew. Chem. Int. Ed.*, 2009, **48**, 2308-2312.
8. G. Ren, D. Hu, E. W. C. Cheng, M. A. Vargas-Reus, P. Reip and R. P. Allaker, *Int. J. Antimicrob. Agents*, 2009, **33**, 587-590.
9. A. Sirelkhatim, S. Mahmud, A. Seeni, N. H. M. Kaus, L. C. Ann, S. K. M. Bakhori, H. Hasan and D. Mohamad, *Nano-Micro Lett.*, 2015, **7**, 219-242.
10. E. Comini, *Anal. Chim. Acta*, 2006, **568**, 28-40.
11. X. Luo, A. Morrin, A. J. Killard and M. R. Smyth, *Electroanalysis*, 2006, **18**, 319-326.
12. R. Koole, E. Groeneveld, D. Vanmaekelbergh, A. Meijerink and C. de Mello Donegá, in *Nanoparticles: Workhorses of Nanoscience*, ed. C. de Mello Donegá, Springer Berlin Heidelberg, Berlin, Heidelberg, 2014, pp. 13-51.
13. H. W. Roesky, I. Haiduc and N. S. Hosmane, *Chem. Rev.*, 2003, **103**, 2579-2596.
14. J. B. Benedict and P. Coppens, *J. Am. Chem. Soc.*, 2010, **132**, 2938-2944.
15. J. A. Libera, J. W. Elam, N. F. Sather, T. Rajh and N. M. Dimitrijevic, *Chem. Mater.*, 2010, **22**, 409-413.
16. A. J. Petrella, H. Deng, N. K. Roberts and R. N. Lamb, *Chem. Mater.*, 2002, **14**, 4339-4342.
17. N. L. Rosi, J. Eckert, M. Eddaoudi, D. T. Vodak, J. Kim, M. O'Keeffe and O. M. Yaghi, *Science*, 2003, **300**, 1127-1129.
18. D. Prochowicz, K. Sokolowski, I. Justyniak, A. Kornowicz, D. Fairen-Jimenez, T. Friscic and J. Lewinski, *Chem. Commun.*, 2015, **51**, 4032-4035.
19. K. Uzarevic, T. C. Wang, S.-Y. Moon, A. M. Fidelli, J. T. Hupp, O. K. Farha and T. Friscic, *Chem. Commun.*, 2016, **52**, 2133-2136.
20. Y.-H. Huang, W.-S. Lo, Y.-W. Kuo, W.-J. Chen, C.-H. Lin and F.-K. Shieh, *Chem. Commun.*, 2017, **53**, 5818-5821.
21. E. Assmann, P. Blaha, R. Laskowski, K. Held, S. Okamoto and G. Sangiovanni, *Phys. Rev. Lett.*, 2013, **110**, 078701.

22. L. E. Smart and E. A. Moore, *Solid State Chemistry: An Introduction*, CRC Press, 4th edn., 2012.
23. K. Samedov, Y. Aksu and M. Driess, *Chem. Eur. J.*, 2012, **18**, 7766-7779.
24. M. Tsaroucha, Y. Aksu, J. D. Epping and M. Driess, *ChemPlusChem*, 2013, **78**, 62-69.
25. S. K. Mandal and H. W. Roesky, *Acc. Chem. Res.*, 2010, **43**, 248-259.
26. K. Manna, P. Ji, F. X. Greene and W. Lin, *J. Am. Chem. Soc.*, 2016, **138**, 7488-7491.
27. H. S. Zijlstra and S. Harder, *Eur. J. Inorg. Chem.*, 2015, **2015**, 19-43.
28. B. Haag, M. Mosrin, H. Ila, V. Malakhov and P. Knochel, *Angew. Chem. Int. Ed.*, 2011, **50**, 9794-9824.
29. E. Weiss, *Angew. Chem. Int. Ed.*, 1993, **32**, 1501-1523.
30. A. C. Hoepker, L. Gupta, Y. Ma, M. F. Faggin and D. B. Collum, *J. Am. Chem. Soc.*, 2011, **133**, 7135-7151.
31. R. E. Mulvey, F. Mongin, M. Uchiyama and Y. Kondo, *Angew. Chem. Int. Ed.*, 2007, **46**, 3802-3824.
32. F. Albert Cotton, Geoffrey Wilkinson, Carlos A. Murillo and M. Bochmann, *Advanced Inorganic Chemistry, 6th Edition*, Wiley-Interscience, New York, 1999.
33. J. Bacsa, F. Hanke, S. Hindley, R. Odedra, G. R. Darling, A. C. Jones and A. Steiner, *Angew. Chem. Int. Ed.*, 2011, **50**, 11685-11687.
34. G. Margraf, H. W. Lerner, M. Bolte and M. Wagner, *Z. Anorg. Allg. Chem.*, 2004, **630**, 217-218.
35. B. Krebs, G. Henkel and M. Dartmann, *Acta Crystallogr. Sect. C*, 1989, **45**, 1010-1012.
36. M. F. Lappert, D. S. Patil and J. B. Pedley, *J. Chem. Soc., Chem. Commun.*, 1975, 830-831.
37. O. I. Guzyr, J. Prust, H. W. Roesky, C. Lehmann, M. Teichert and F. Cimpoesu, *Organometallics*, 2000, **19**, 1549-1555.
38. S. G. Blanco, M. P. G. Sal, S. M. Carreras, M. Mena, P. Royo and R. Serrano, *J. Chem. Soc., Chem. Commun.*, 1986, 1572-1573.
39. H. Eriksson and M. Håkansson, *Organometallics*, 1997, **16**, 4243-4244.
40. D. R. Armstrong, A. R. Kennedy, R. E. Mulvey, J. A. Parkinson and S. D. Robertson, *Chem. Sci.*, 2012, **3**, 2700-2707.
41. M. Westerhausen, *Inorg. Chem.*, 1991, **30**, 96-101.
42. M. Westerhausen, *Dalton Trans.*, 2006, 4755-4768.
43. N. Y. Turova, E. P. Turevskaya, V. G. Kessler and M. I. Yanovskaya, *The Chemistry of Metal Alkoxides, Chapters 9-10*, Springer, 2002.
44. H. W. Roesky, M. G. Walawalkar and R. Murugavel, *Acc. Chem. Res.*, 2001, **34**, 201-211.
45. J. Lewiński, Z. Ochal, E. Bojarski, E. Tratkiewicz, I. Justyniak and J. Lipkowski, *Angew. Chem. Int. Ed.*, 2003, **42**, 4643-4646.
46. J. Lewiński, W. Marciniak, J. Lipkowski and I. Justyniak, *J. Am. Chem. Soc.*, 2003, **125**, 12698-12699.
47. J. Lewiński, W. Śliwiński, M. Dranka, I. Justyniak and J. Lipkowski, *Angew. Chem. Int. Ed.*, 2006, **45**, 4826-4829.
48. P. Sobota, R. Petrus, K. Zelga, L. Makolski, D. Kubicki and J. Lewinski, *Chem. Commun.*, 2013, **49**, 10477-10479.
49. M. B. Smith and J. March, *March's Advanced Organic Chemistry: Reactions, Mechanisms and Structure*, John Wiley & Sons, Inc., Hoboken, New Jersey, Sixth Edition edn., 2007.
50. D. Nobuto and M. Uchiyama, *J. Org. Chem.*, 2008, **73**, 1117-1120.
51. B. Sharma, T. M. Callaway, A. C. Lamb, C. A. Steren, S.-J. Chen and Z.-L. Xue, *Inorg. Chem.*, 2013, **52**, 11409-11421.
52. J. B. Miller, J. Schwartz and S. L. Bernasek, *J. Am. Chem. Soc.*, 1993, **115**, 8239-8247.
53. U. Schubert, *J. Mater. Chem.*, 2005, **15**, 3701-3715.
54. W. Reeve, C. M. Erikson and P. F. Aluotto, *Can. J. Chem.*, 1979, **57**, 2747-2754.
55. J. Storre, A. Klemp, H. W. Roesky, H.-G. Schmidt, M. Noltemeyer, R. Fleischer and D. Stalke, *J. Am. Chem. Soc.*, 1996, **118**, 1380-1386.
56. A. F. Dunlop-Brière and M. C. Baird, *Organometallics*, 2010, **29**, 6117-6120.
57. A. Conde, R. Fandos, A. Otero and A. Rodríguez, *Organometallics*, 2007, **26**, 1568-1570.
58. W. A. Herrmann, R. W. Fischer, W. Scherer and M. U. Rauch, *Angew. Chem. Int. Ed.*, 1993, **32**, 1157-1160.
59. M. Safa, M. C. Jennings and R. J. Puddephatt, *Organometallics*, 2012, **31**, 3539-3550.
60. M. Veith, *Chem. Rev.*, 1990, **90**, 3-16.
61. A. T. Wagner and P. W. Roesky, *Eur. J. Inorg. Chem.*, 2016, **2016**, 782-791.
62. A. Styskalik, D. Skoda, C. Barnes and J. Pinkas, *Catalysts*, 2017, **7**, 168.
63. J. Lewiński, W. Bury, I. Justyniak and J. Lipkowski, *Angew. Chem. Int. Ed.*, 2006, **45**, 2872-2875.
64. S. J. Obrey, S. G. Bott and A. R. Barron, *Organometallics*, 2001, **20**, 5162-5170.
65. I. Feinstein-Jaffe, D. Gibson, S. J. Lippard, R. R. Schrock and A. Spool, *J. Am. Chem. Soc.*, 1984, **106**, 6305-6310.
66. Y. Champouret, Y. Coppel and M. L. Kahn, *J. Am. Chem. Soc.*, 2016, **138**, 16322-16328.
67. A. Glaria, M. L. Kahn, T. Cardinal, F. Senocq, V. Jubera and B. Chaudret, *New J. Chem.*, 2008, **32**, 662-669.
68. P. Arnal, R. J. P. Corriu, D. Leclercq, P. H. Mutin and A. Vioux, *J. Mater. Chem.*, 1996, **6**, 1925-1932.
69. A. Vioux, *Chem. Mater.*, 1997, **9**, 2292-2299.
70. A. R. Barron, *Comments Inorg. Chem.*, 1993, **14**, 123-153.
71. D. Chakraborty and E. Y. X. Chen, *Organometallics*, 2003, **22**, 207-210.
72. M. R. Mason, J. M. Smith, S. G. Bott and A. R. Barron, *J. Am. Chem. Soc.*, 1993, **115**, 4971-4984.
73. C. J. Harlan, M. R. Mason and A. R. Barron, *Organometallics*, 1994, **13**, 2957-2969.
74. C. J. Harlan, E. G. Gillan, S. G. Bott and A. R. Barron, *Organometallics*, 1996, **15**, 5479-5488.
75. R. M. McKinlay, S. J. Dalgarno, P. J. Nichols, S. Papadopoulos, J. L. Atwood and C. L. Raston, *Chem. Commun.*, 2007, 2393-2395.
76. C. C. Landry, C. J. Harlan, S. G. Bott and A. R. Barron, *Angew. Chem. Int. Ed.*, 1995, **34**, 1201-1202.
77. A. Walz, M. Niemeyer and J. Weidlein, *Z. Anorg. Allg. Chem.*, 1999, **625**, 547-549.
78. J. Storre, A. Klemp, H. W. Roesky, R. Fleischer and D. Stalke, *Organometallics*, 1997, **16**, 3074-3076.
79. M. E. Kenney and A. W. Laubengayer, *J. Am. Chem. Soc.*, 1954, **76**, 4839-4841.
80. P. J. Nichols, S. Papadopoulos and C. L. Raston, *Chem. Commun.*, 2000, 1227-1228.
81. W. Kuran and M. Czernecka, *J. Organomet. Chem.*, 1984, **263**, 1-7.
82. D. Prochowicz, K. Sokołowski and J. Lewiński, *Coord. Chem. Rev.*, 2014, **270–271**, 112-126.
83. W. Bury, E. Krajewska, M. Dutkiewicz, K. Sokolowski, I. Justyniak, Z. Kaszkur, K. J. Kurzydlowski, T. Plocinski and J. Lewinski, *Chem. Commun.*, 2011, **47**, 5467-5469.
84. G. Prabusankar, B. Jousseaume, T. Toupance and H. Allouchi, *Angew. Chem. Int. Ed.*, 2006, **45**, 1255-1258.

85. P. Jaumier, B. Jousscaume, P. Jaumier, M. Lahcini, F. Ribot and C. Sanchez, *Chem. Commun.*, 1998, 369-370.
86. I. Feinstein-Jaffe, S. F. Pedersen and R. R. Schrock, *J. Am. Chem. Soc.*, 1983, **105**, 7176-7177.
87. B. A. Dougan and Z.-L. Xue, *Sci. China Chem.*, 2011, **54**, 1903-1908.
88. P. Chen, L. Zhang, Z.-L. Xue, Y.-D. Wu and X. Zhang, *Inorg. Chem.*, 2017, **56**, 7111-7119.
89. G. Schoettel, J. Kress, J. Fischer and J. A. Osborn, *J. Chem. Soc., Chem. Commun.*, 1988, 914-915.
90. S.-J. Chen, J. K. C. Abbott, C. A. Steren and Z.-L. Xue, *J. Cluster Sci.*, 2010, **21**, 325-337.
91. J. L. Krinsky, L. L. Anderson, J. Arnold and R. G. Bergman, *Inorg. Chem.*, 2008, **47**, 1053-1066.
92. F. Banse, F. Ribot, P. Toledano, J. Maquet and C. Sanchez, *Inorg. Chem.*, 1995, **34**, 6371-6379.
93. R. Marschall and L. Wang, *Catal. Today*, 2014, **225**, 111-135.
94. N. Y. Turova, *Russ. Chem. Rev.*, 2004, **73**, 1041-1064.
95. V. W. Day, T. A. Eberspacher, Y. Chen, J. Hao and W. G. Klemperer, *Inorg. Chim. Acta*, 1995, **229**, 391-405.
96. S. D. Pike, E. R. White, M. S. P. Shaffer and C. K. Williams, *Nat. Commun.*, 2016, **7**, 13008.
97. V. G. Kessler, G. I. Spijksma, G. A. Seisenbaeva, S. Håkansson, D. H. A. Blank and H. J. M. Bouwmeester, *J. Sol-Gel Sci. Technol.*, 2006, **40**, 163-179.
98. F. R. Kogler, M. Jupa, M. Puchberger and U. Schubert, *J. Mater. Chem.*, 2004, **14**, 3133-3138.
99. U. Schubert, *Coord. Chem. Rev.*, 2017, **350**, 61-67.
100. G. A. Seisenbaeva, V. G. Kessler, R. Pazik and W. Strek, *Dalton Trans.*, 2008, 3412-3421.
101. C. G. Lugmair, T. D. Tilley and A. L. Rheingold, *Chem. Mater.*, 1997, **9**, 339-348.
102. P. F. Haywood, M. R. Hill, N. K. Roberts, D. C. Craig, J. J. Russell and R. N. Lamb, *Eur. J. Inorg. Chem.*, 2008, **2008**, 2024-2032.
103. W. Bury, I. Justyniak, D. Prochowicz, A. Rola-Noworyta and J. Lewiński, *Inorg. Chem.*, 2012, **51**, 7410-7414.
104. W. Bury, I. Justyniak, D. Prochowicz, Z. Wrobel and J. Lewinski, *Chem. Commun.*, 2012, **48**, 7362-7364.
105. M. K. Leszczynski, I. Justyniak, K. Zelga and J. Lewinski, *Dalton Trans.*, 2017, **46**, 12404-12407.
106. M.-T. Chen and C.-T. Chen, *Dalton Trans.*, 2017, **46**, 10181-10184.
107. R. Boomishankar, P. I. Richards and A. Steiner, *Angew. Chem. Int. Ed.*, 2006, **45**, 4632-4634.
108. F. R. Fronczek, E. C. Baker, P. R. Sharp, K. N. Raymond, H. G. Alt and M. D. Rausch, *Inorg. Chem.*, 1976, **15**, 2284-2289.
109. W. E. Hunter, D. C. Hrncir, R. V. Bynum, R. A. Penttila and J. L. Atwood, *Organometallics*, 1983, **2**, 750-755.
110. P. Ghosh and G. Parkin, *Inorg. Chem.*, 1996, **35**, 1429-1430.
111. A. Drąg-Jarząbek, R. Petrus and P. Sobota, *Inorg. Chem.*, 2016, **55**, 9524-9527.
112. F. Rominger, A. Müller and U. Thewalt, *Chem. Ber.*, 1994, **127**, 797-804.
113. L. F. Sánchez-Barba, D. L. Hughes, S. M. Humphrey and M. Bochmann, *Organometallics*, 2006, **25**, 1012-1020.
114. W. Teng, M. Guino-o, J. Hitzbleck, U. Englich and K. Ruhlandt-Senge, *Inorg. Chem.*, 2006, **45**, 9531-9539.
115. S. Sarish, S. Nembenna, S. Nagendran, H. W. Roesky, A. Pal, R. Herbst-Irmer, A. Ringe and J. Magull, *Inorg. Chem.*, 2008, **47**, 5971-5977.
116. R. Murugavel, V. Chandrasekhar and H. W. Roesky, *Acc. Chem. Res.*, 1996, **29**, 183-189.
117. O. Michel, S. König, K. W. Törnroos, C. Maichle-Mössmer and R. Anwander, *Chem. Eur. J.*, 2011, **17**, 11857-11867.
118. K. W. Terry, C. G. Lugmair and T. D. Tilley, *J. Am. Chem. Soc.*, 1997, **119**, 9745-9756.
119. A. Martín, M. Mena, M. d. C. Morales-Varela and C. Santamaría, *Eur. J. Inorg. Chem.*, 2006, **2006**, 2137-2145.
120. A. Martín, M. Mena, María del C. Morales-Varela and C. Santamaría, *Eur. J. Inorg. Chem.*, 2004, **2004**, 1914-1921.
121. L. H. van Poppel, S. G. Bott and A. R. Barron, *Polyhedron*, 2003, **22**, 9-17.
122. J. Bareš, Z. Padělková, P. Meunier, N. Pirio and A. Růžička, *J. Organomet. Chem.*, 2009, **694**, 1263-1265.
123. A. M. Drummond, L. T. Gibson, A. R. Kennedy, R. E. Mulvey, C. T. O'Hara, R. B. Rowlings and T. Weightman, *Angew. Chem. Int. Ed.*, 2002, **41**, 2382-2384.
124. A. R. Kennedy, R. E. Mulvey and R. B. Rowlings, *Angew. Chem. Int. Ed.*, 1998, **37**, 3180-3183.
125. P. Sobota, J. Utko, T. Lis, Ł. John, R. Petrus and A. Drąg-Jarząbek, *Inorg. Chem.*, 2016, **55**, 4636-4642.
126. E. M. Goggins, T. T. Lekich, W. W. Weare, R. D. Sommer, M. A. Ribeiro and C. B. Pinheiro, *Eur. J. Inorg. Chem.*, 2016, **2016**, 1054-1059.
127. S. Nembenna, H. W. Roesky, S. K. Mandal, R. B. Oswald, A. Pal, R. Herbst-Irmer, M. Noltemeyer and H.-G. Schmidt, *J. Am. Chem. Soc.*, 2006, **128**, 13056-13057.
128. S. P. Sarish, S. Nembenna, H. W. Roesky, H. Ott, A. Pal, D. Stalke, S. Dutta and S. K. Pati, *Angew. Chem. Int. Ed.*, 2009, **48**, 8740-8742.
129. P. M. Gurubasavaraj, S. K. Mandal, H. W. Roesky, R. B. Oswald, A. Pal and M. Noltemeyer, *Inorg. Chem.*, 2007, **46**, 1056-1061.
130. S. K. Mandal, P. M. Gurubasavaraj, H. W. Roesky, R. B. Oswald, J. Magull and A. Ringe, *Inorg. Chem.*, 2007, **46**, 7594-7600.
131. B. Li, C. Zhang, Y. Yang, H. Zhu and H. W. Roesky, *Inorg. Chem.*, 2015, **54**, 6641-6646.
132. S. Schulz, J. Spielmann, D. Blaser and C. Wolper, *Chem. Commun.*, 2011, **47**, 2676-2678.
133. J. Garcia-Rios, R. F. Hernandez-Campos, F. Rascon-Cruz, V. A. Moreno-Martinez, R. Huerta-Lavorie, M.-A. Velazquez-Carmona, R. Cea-Olivares, D. Martinez-Otero and V. Jancik, *RSC Adv.*, 2015, **5**, 99722-99731.
134. S. Nembenna, S. Singh, A. Jana, H. W. Roesky, Y. Yang, H. Ye, H. Ott and D. Stalke, *Inorg. Chem.*, 2009, **48**, 2273-2276.
135. Y. Yang, T. Schulz, M. John, Z. Yang, V. M. Jiménez-Pérez, H. W. Roesky, P. M. Gurubasavaraj, D. Stalke and H. Ye, *Organometallics*, 2008, **27**, 769-777.
136. S. Singh, S. S. Kumar, V. Chandrasekhar, H.-J. Ahn, M. Biadene, H. W. Roesky, N. S. Hosmane, M. Noltemeyer and H.-G. Schmidt, *Angew. Chem. Int. Ed.*, 2004, **43**, 4940-4943.
137. C. Boulho, H. S. Zijlstra, A. Hofmann, P. H. M. Budzelaar and S. Harder, *Chem. Eur. J.*, 2016, **22**, 17450-17459.
138. G. Bai, Y. Peng, H. W. Roesky, J. Li, H.-G. Schmidt and M. Noltemeyer, *Angew. Chem. Int. Ed.*, 2003, **42**, 1132-1135.
139. G. Bai, H. W. Roesky, J. Li, M. Noltemeyer and H.-G. Schmidt, *Angew. Chem. Int. Ed.*, 2003, **42**, 5502-5506.
140. G. Bai, S. Singh, H. W. Roesky, M. Noltemeyer and H.-G. Schmidt, *J. Am. Chem. Soc.*, 2005, **127**, 3449-3455.
141. V. Jancik, L. W. Pineda, J. Pinkas, H. W. Roesky, D. Neculai, A. M. Neculai and R. Herbst-Irmer, *Angew. Chem. Int. Ed.*, 2004, **43**, 2142-2145.
142. S. González-Gallardo, V. Jancik, R. Cea-Olivares, R. A. Toscano and M. Moya-Cabrera, *Angew. Chem. Int. Ed.*, 2007, **46**, 2895-2898.

143. S. Singh, V. Jancik, H. W. Roesky and R. Herbst-Irmer, *Inorg. Chem.*, 2006, **45**, 949-951.
144. M. H. Feng and K. J. Chao, *J. Mol. Struct.*, 1996, **364**, 51-57.
145. F. C. Jentoft, *Advances in Catalysis, Volume 57*, Academic Press, 2014.
146. G. B. Nikiforov, H. W. Roesky, T. Schulz, D. Stalke and M. Witt, *Inorg. Chem.*, 2008, **47**, 6435-6443.
147. R. Huerta-Lavorie, F. Rascón-Cruz, D. Solis-Ibarra, N. Zavala-Segovia and V. Jancik, *Eur. J. Inorg. Chem.*, 2011, **2011**, 4795-4799.
148. P. M. Gurubasavaraj, H. W. Roesky, B. Nekoueishahraki, A. Pal and R. Herbst-Irmer, *Inorg. Chem.*, 2008, **47**, 5324-5331.
149. G. B. Nikiforov, H. W. Roesky, P. G. Jones, R. B. Oswald and M. Noltemeyer, *Dalton Trans.*, 2007, 4149-4159.
150. M. Veith, H. Hreleva-Carparrotti and V. Huch, *J. Organomet. Chem.*, 2007, **692**, 2784-2788.
151. M. Veith, H. Hreleva, M. Gasthauer, A. Rammo and V. Huch, *Z. Anorg. Allg. Chem.*, 2006, **632**, 985-991.
152. E. Bernabé-Pablo, V. Jancik and M. Moya-Cabrera, *Inorg. Chem.*, 2013, **52**, 6944-6950.
153. P. M. Gurubasavaraj, H. W. Roesky, P. M. V. Sharma, R. B. Oswald, V. Dolle, R. Herbst-Irmer and A. Pal, *Organometallics*, 2007, **26**, 3346-3351.
154. G. L. Hillhouse and J. E. Bercaw, *J. Am. Chem. Soc.*, 1984, **106**, 5472-5478.
155. C. Boulho, H. S. Zijlstra and S. Harder, *Eur. J. Inorg. Chem.*, 2015, **2015**, 2132-2138.
156. A. Mukherjee, S. Nembenna, T. K. Sen, S. P. Sarish, P. K. Ghorai, H. Ott, D. Stalke, S. K. Mandal and H. W. Roesky, *Angew. Chem. Int. Ed.*, 2011, **50**, 3968-3972.
157. S. K. Mandal, P. M. Gurubasavaraj, H. W. Roesky, G. Schwab, D. Stalke, R. B. Oswald and V. Dolle, *Inorg. Chem.*, 2007, **46**, 10158-10167.
158. K. R. Campos, A. Klapars, J. H. Waldman, P. G. Dormer and C.-y. Chen, *J. Am. Chem. Soc.*, 2006, **128**, 3538-3539.
159. M. Tsaroucha, Y. Aksu, E. Irran and M. Driess, *Chem. Mater.*, 2011, **23**, 2428-2438.
160. S. U. Ghazi, R. Kumar, M. J. Heeg and J. P. Oliver, *Inorg. Chem.*, 1994, **33**, 411-414.
161. A. McLaren, T. Valdes-Solis, G. Li and S. C. Tsang, *J. Am. Chem. Soc.*, 2009, **131**, 12540-12541.
162. S. Tian, F. Yang, D. Zeng and C. Xie, *J. Phys. Chem. C*, 2012, **116**, 10586-10591.
163. M. Niederberger and N. Pinna, in *Metal Oxide Nanoparticles in Organic Solvents. Synthesis, Formation, Assembly and Application*, Springer, 2009, ch. 2.
164. A. E. Danks, S. R. Hall and Z. Schnepp, *Mater. Horizons*, 2016, **3**, 91-112.
165. D. Levy and M. Zayat, *The Sol-Gel Handbook - Synthesis, Characterization, and Applications: Synthesis, Characterization and Applications, 3-Volume Set*, Wiley, 2015.
166. A. Glaria, M. L. Kahn, A. Falqui, P. Lecante, V. Collière, M. Respaud and B. Chaudret, *ChemPhysChem*, 2008, **9**, 2035-2041.
167. G. Casterou , V. Collière, P. Lecante, Y. Coppel, P.-A. Eliat, F. Gauffre and M. L. Kahn, *Chem. Eur. J.*, 2015, **21**, 18855-18861.
168. A. Glaria, M. L. Kahn, P. Lecante, B. Barbara and B. Chaudret, *ChemPhysChem*, 2008, **9**, 776-780.
169. A. Glaria, M. L. Kahn, B. Chaudret, P. Lecante, M.-J. Casanove and B. Barbara, *Mater. Chem. Phys.*, 2011, **129**, 605-610.
170. N. Cordente, B. Toustou, V. Collière, C. Amiens, B. Chaudret, M. Verelst, M. Respaud and J.-M. Broto, *C.R. Acad. Sci., Ser. IIc: Chim.*, 2001, **4**, 143-148.
171. S. D. Pike, E. R. White, A. Regoutz, N. Sammy, D. J. Payne, C. K. Williams and M. S. P. Shaffer, *ACS Nano*, 2017, **11**, 2714-2723.
172. J. Jońca, A. Ryzhikov, S. Palussière, J. Esvan, K. Fajerwerg, P. Menini, M. L. Kahn and P. Fau, *ChemPhysChem*, 2017, **18**, 2658-2665.
173. N. J. Brown, J. Weiner, K. Hellgardt, M. S. P. Shaffer and C. K. Williams, *Chem. Commun.*, 2013, **49**, 11074-11076.
174. K. L. Orchard, M. S. P. Shaffer and C. K. Williams, *Chem. Mater.*, 2012, **24**, 2443-2448.
175. T. V. Richter, F. Schüler, R. Thomann, R. Mülhaupt and S. Ludwigs, *Macromol. Rapid Commun.*, 2009, **30**, 579-583.
176. J. Paczesny, M. Wolska-Pietkiewicz, I. Binkiewicz, Z. Wróbel, M. Wadowska, K. Matuła, I. Dzięcielewski, D. Pociecha, J. Smalc-Koziorowska, J. Lewiński and R. Hołyst, *Chem. Eur. J.*, 2015, **21**, 16941-16947.
177. A. Grala, M. Wolska-Pietkiewicz, W. Danowski, Z. Wrobel, J. Grzonka and J. Lewinski, *Chem. Commun.*, 2016, **52**, 7340-7343.
178. M. Wolska-Pietkiewicz, A. Grala, I. Justyniak, D. Hryciuk, M. Jędrzejewska, J. Grzonka, K. J. Kurzydłowski and J. Lewiński, *Chem. Eur. J.*, 2017, **23**, 11856-11865.
179. J. Lewinski, M. Wolska-Pietkiewicz, K. Tokarska, A. Grala, A. Wojewódzka, E. Chwojnowska, J. Grzonka, P. Cywiński, K. Kruczała, Z. Sojka and M. Chudy, *Chem. Eur. J.*, 2018, Accepted Article.
180. A. M. Cieślak, M. V. Pavliuk, L. D'Amario, M. Abdellah, K. Sokołowski, U. Rybinska, D. L. A. Fernandes, M. K. Leszczyński, F. Mamedov, A. M. El-Zhory, J. Föhlinger, A. Budinská, M. Wolska-Pietkiewicz, L. Hammarström, J. Lewiński and J. Sá, *Nano Energy*, 2016, **30**, 187-192.
181. E. Chwojnowska, M. Wolska-Pietkiewicz, J. Grzonka and J. Lewinski, *Nanoscale*, 2017, **9**, 14782-14786.
182. J. Paczesny, M. Wolska-Pietkiewicz, I. Binkiewicz, M. Wadowska, Z. Wróbel, K. Matuła, W. Nogala, J. Lewiński and R. Hołyst, *ACS Applied Materials & Interfaces*, 2016, **8**, 13532-13541.
183. M. V. Pavliuk, A. M. Cieslak, M. Abdellah, A. Budinska, S. Pullen, K. Sokolowski, D. L. A. Fernandes, J. Szlachetko, E. L. Bastos, S. Ott, L. Hammarstrom, T. Edvinsson, J. Lewinski and J. Sa, *Sustainable Energy & Fuels*, 2017, **1**, 69-73.
184. M. L. Kahn, M. Monge, V. Collière, F. Senocq, A. Maisonnat and B. Chaudret, *Adv. Funct. Mater.*, 2005, **15**, 458-468.
185. M. Monge, M. L. Kahn, A. Maisonnat and B. Chaudret, *Angew. Chem. Int. Ed.*, 2003, **42**, 5321-5324.
186. J. Rubio-Garcia, Y. Coppel, P. Lecante, C. Mingotaud, B. Chaudret, F. Gauffre and M. L. Kahn, *Chem. Commun.*, 2011, **47**, 988-990.
187. S. Saliba, C. Valverde Serrano, J. Keilitz, M. L. Kahn, C. Mingotaud, R. Haag and J.-D. Marty, *Chem. Mater.*, 2010, **22**, 6301-6309.
188. Z. Zheng, R. Butynska, C. V. Serrano, J.-D. Marty, C. Mingotaud and M. L. Kahn, *Chem. Eur. J.*, 2016, **22**, 15614-15618.
189. B. Luo, J. E. Rossini and W. L. Gladfelter, *Langmuir*, 2009, **25**, 13133-13141.
190. S. Daniele, M. N. Ghazzal, L. G. Hubert-Pfalzgraf, C. Duchamp, C. Guillard and G. Ledoux, *Mater. Res. Bull.*, 2006, **41**, 2210-2218.
191. T. J. Boyle, S. D. Bunge, N. L. Andrews, L. E. Matzen, K. Sieg, M. A. Rodriguez and T. J. Headley, *Chem. Mater.*, 2004, **16**, 3279-3288.
192. C. Lizandara-Pueyo, S. Siroky, M. R. Wagner, A. Hoffmann, J. S. Reparaz, M. Lehmann and S. Polarz, *Adv. Funct. Mater.*, 2011, **21**, 295-304.
193. C. Lizandara-Pueyo, M. W. E. van den Berg, A. De Toni, T. Goes and S. Polarz, *J. Am. Chem. Soc.*, 2008, **130**, 16601-16610.

194. J. Jońca, A. Ryzhikov, K. Fajerwerg, M. L. Kahn, B. Chaudret, A. Chapelle, P. Menini and P. Fau, *Procedia Eng.*, 2014, **87**, 923-926.
195. J. Jońca, A. Ryzhikov, M. L. Kahn, K. Fajerwerg, A. Chapelle, P. Menini and P. Fau, *Chem. Eur. J.*, 2016, **22**, 10127-10135.
196. V. Ischenko, S. Polarz, D. Grote, V. Stavarache, K. Fink and M. Driess, *Adv. Funct. Mater.*, 2005, **15**, 1945-1954.
197. S. Polarz, J. Strunk, V. Ischenko, M. W. E. van den Berg, O. Hinrichsen, M. Muhler and M. Driess, *Angew. Chem. Int. Ed.*, 2006, **45**, 2965-2969.
198. C. Lizandara Pueyo, S. Siroky, S. Landsmann, M. W. E. van den Berg, M. R. Wagner, J. S. Reparaz, A. Hoffmann and S. Polarz, *Chem. Mater.*, 2010, **22**, 4263-4270.
199. L. Chen, J. Xu, D. A. Tanner, R. Phelan, M. Van der Meulen, J. D. Holmes and M. A. Morris, *Chem. Eur. J.*, 2009, **15**, 440-448.
200. L. Chen, K. Rahme, J. D. Holmes, M. A. Morris and N. K. Slater, *Nanoscale Res. Lett.*, 2012, **7**, 297.
201. S. Lee and A. Sardesai, *Top. Catal.*, 2005, **32**, 197-207.
202. S. D. Pike, A. Garcia-Trenco, E. R. White, A. H. M. Leung, J. Weiner, M. S. P. Shaffer and C. K. Williams, *Catal. Sci. Technol.*, 2017, **7**, 3842-3850.
203. Y. Coppel, G. Spataro, C. Pages, B. Chaudret, A. Maisonnat and M. L. Kahn, *Chem. Eur. J.*, 2012, **18**, 5384-5393.
204. C. N. Valdez, A. M. Schimpf, D. R. Gamelin and J. M. Mayer, *ACS Nano*, 2014, **8**, 9463-9470.
205. I. P. Silverwood, C. W. Keyworth, N. J. Brown, M. S. P. Shaffer, C. K. Williams, K. Hellgardt, G. H. Kelsall and S. G. Kazarian, *Appl. Spectrosc.*, 2014, **68**, 88-94.
206. A. Garcia-Trenco, E. R. White, M. S. P. Shaffer and C. K. Williams, *Catal. Sci. Technol.*, 2016, **6**, 4389-4397.
207. N. J. Brown, A. García-Trenco, J. Weiner, E. R. White, M. Allinson, Y. Chen, P. P. Wells, E. K. Gibson, K. Hellgardt, M. S. P. Shaffer and C. K. Williams, *ACS Catal.*, 2015, **5**, 2895-2902.
208. S. Noimark, J. Weiner, N. Noor, E. Allan, C. K. Williams, M. S. P. Shaffer and I. P. Parkin, *Adv. Funct. Mater.*, 2015, **25**, 1367-1373.
209. S. K. Sehmi, S. Noimark, S. D. Pike, J. C. Bear, W. J. Peveler, C. K. Williams, M. S. P. Shaffer, E. Allan, I. P. Parkin and A. J. MacRobert, *ACS Omega*, 2016, **1**, 334-343.
210. M. Krumm, C. L. Pueyo and S. Polarz, *Chem. Mater.*, 2010, **22**, 5129-5136.
211. A. Ryzhikov, J. Jońca, M. Kahn, K. Fajerwerg, B. Chaudret, A. Chapelle, P. Ménini, C. H. Shim, A. Gaudon and P. Fau, *J. Nanopart. Res.*, 2015, **17**, 280.
212. J. Carrey, H. Carrère, M. L. Kahn, B. Chaudret, X. Marie and M. Respaud, *Semicond. Sci. Technol.*, 2008, **23**, 025003.
213. S. Polarz, F. Neues, M. W. E. van den Berg, W. Grünert and L. Khodeir, *J. Am. Chem. Soc.*, 2005, **127**, 12028-12034.
214. W. J. E. Beek, L. H. Slooff, M. M. Wienk, J. M. Kroon and R. A. J. Janssen, *Adv. Funct. Mater.*, 2005, **15**, 1703-1707.
215. A. Gonzalez-Campo, K. L. Orchard, N. Sato, M. S. P. Shaffer and C. K. Williams, *Chem. Commun.*, 2009, 4034-4036.
216. S. Saliba, Y. Coppel, M.-F. Achard, C. Mingotaud, J.-D. Marty and M. L. Kahn, *Angew. Chem. Int. Ed.*, 2011, **50**, 12032-12035.
217. J. Lewinski, W. Marciniak, J. Lipkowski and I. Justyniak, *J. Am. Chem. Soc.*, 2003, **125**, 12698-12699.
218. M. Haakansson, M. Oertendahl, S. Jagner, M. P. Sigalas and O. Eisenstein, *Inorg. Chem.*, 1993, **32**, 2018-2024.
219. K. Sokołowski, I. Justyniak, W. Bury, J. Grzonka, Z. Kaszkur, Ł. Mąkolski, M. Dutkiewicz, A. Lewalska, E. Krajewska, D. Kubicki, K. Wójcik, K. J. Kurzydłowski and J. Lewiński, *Chem. Eur. J.*, 2015, **21**, 5488-5495.
220. S. Polarz, C. L. Pueyo and M. Krumm, *Inorg. Chim. Acta*, 2010, **363**, 4148-4157.
221. M. Voggenreiter, P. Vöpel, B. Smarsly and S. Polarz, *Z. Anorg. Allg. Chem.*, 2017, **643**, 93-100.
222. M. L. Kahn, A. Glaria, C. Pages, M. Monge, L. Saint Macary, A. Maisonnat and B. Chaudret, *J. Mater. Chem.*, 2009, **19**, 4044-4060.
223. C. Pagès, Y. Coppel, M. L. Kahn, A. Maisonnat and B. Chaudret, *ChemPhysChem*, 2009, **10**, 2334-2344.
224. J. G. Smith and P. K. Jain, *J. Am. Chem. Soc.*, 2016, **138**, 6765-6773.
225. T. Chen and V. O. Rodionov, *ACS Catal.*, 2016, **6**, 4025-4033.
226. S. Campisi, M. Schiavoni, C. Chan-Thaw and A. Villa, *Catalysts*, 2016, **6**, 185.
227. S. M. Ansar and C. L. Kitchens, *ACS Catal.*, 2016, **6**, 5553-5560.
228. P. Haider, A. Urakawa, E. Schmidt and A. Baiker, *J. Mol. Catal. A: Chem.*, 2009, **305**, 161-169.
229. K. L. Orchard, A. J. P. White, M. S. P. Shaffer and C. K. Williams, *Organometallics*, 2009, **28**, 5828-5832.
230. K. L. Orchard, J. E. Harris, A. J. P. White, M. S. P. Shaffer and C. K. Williams, *Organometallics*, 2011, **30**, 2223-2229.
231. A. M. Schimpf, C. E. Gunthardt, J. D. Rinehart, J. M. Mayer and D. R. Gamelin, *J. Am. Chem. Soc.*, 2013, **135**, 16569-16577.
232. C. Lizandara-Pueyo, S. Dilger, M. R. Wagner, M. Gerigk, A. Hoffmann and S. Polarz, *CrystEngComm*, 2014, **16**, 1525-1531.
233. M. R. Hill, J. J. Russell and R. N. Lamb, *Chem. Mater.*, 2008, **20**, 2461-2467.
234. M. I. Yanovskaya, E. P. Turevskaya, V. G. Kessler, I. E. Obvintseva and N. Y. Turova, *Integr. Ferroelectr.*, 1992, **1**, 343-352.
235. J. H. Shim, C.-C. Chao, H. Huang and F. B. Prinz, *Chem. Mater.*, 2007, **19**, 3850-3854.

View Article Online
DOI: 10.1039/C8DT00017D

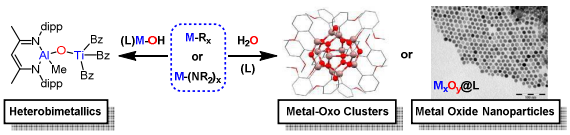

Organometallic and metal amide reagents react with -OH groups to generate metal-oxygen connectivity yielding metal-oxo heterobimetallics, clusters and nanoparticles